nature neuroscience

Resource

https://doi.org/10.1038/s41593-025-01919-0

Projectome-based characterization of hypothalamic peptidergic neurons in male mice

Received: 27 April 2023

Accepted: 7 February 2025

Published online: 26 March 2025

Check for updates

A list of authors and their affiliations appears at the end of the paper

The hypothalamus coordinately regulates physiological homeostasis and innate behaviors, yet the detailed arrangement of hypothalamic axons remains unclear. Here we mapped the whole-brain projections of over 7,000 hypothalamic neurons expressing distinct neuropeptides in male mice, identifying 2 main classes and 31 types using single-neuron projectome analysis. These classes/types exhibited regionally biased soma distribution and specific neuropeptide enrichment. Notably, many projectome types extended long-range axon collaterals to distinct brain regions, allowing single axons to co-regulate multiple targets. We uncovered topographic organization of certain peptidergic axons at specific targets, along with diverse single-neuron projectome patterns in *Orexin*, *Agrp* and *Pomc* populations. Furthermore, hypothalamic peptidergic neurons showed correlated innervation of subdomains in the periaqueductal gray and organized into modular subnetworks within the hypothalamus, providing a structural basis for coordinated outputs. This dataset highlights the complexity of hypothalamic axonal projections and lays a foundation for future investigation of the circuit mechanisms underlying hypothalamic functions.

The hypothalamus, located at the ventral base of the brain, is an evolutionarily conserved structure comprising numerous nuclei and interconnected neurons[1–4]. It coordinately regulates neuroendocrine, autonomic and somatomotor responses crucial for maintaining vital behaviors and physiological balance. Hypothalamic control of behaviors and physiology relies on evolutionarily conserved neuropeptides[5,6]. Despite their recognized importance, the axonal projections of hypothalamic peptidergic neurons remain incompletely understood.

Previous studies used anterograde tracers such as *Phaseolus vulgaris* leucoagglutinin (PHL) to map projections from specific hypothalamic nuclei, revealing extensive brain-wide and intra-hypothalamic connections[7–14]. Although informative, these studies could not distinguish projections of distinct peptidergic populations within the same nucleus. Recently, virus-mediated anterograde tracing has delineated projections of hypothalamic neurons expressing distinct neuropeptides[15–17], but these bulk tracing methods could not reveal projections of individual neurons, particularly targets innervated by collaterals from the same axon. Notably, manipulating specific hypothalamic peptidergic populations often affects multiple behaviors and physiological processes[18,19], suggesting their complexity and heterogeneity.

Recent advancements in single-cell transcriptome analysis have revealed the extensive molecular diversity of hypothalamic peptidergic neurons[20–22]. However, there is a notable lack of characterization of axonal projection patterns of hypothalamic peptidergic neurons at a scale or resolution similar to that of single-cell transcriptome analysis. We contend that hypothalamic neurons with similar transcription profiles may serve distinct functions by projecting to distinct downstream targets (divergence). Conversely, neurons differing in transcription profiles may engage in similar biological functions by targeting the

e-mail: ydsun@ion.ac.cn; sxu@ion.ac.cn; huigong@brainsmatics.org; yangang.sun@ion.ac.cn; xiaohongxu46@gmail.com

same downstream (convergence). Thus, comprehensive mapping of the whole-brain projection patterns (projectomes) of individual hypothalamic axons is crucial for understanding the molecular, cellular and circuit architecture underlying hypothalamic functions. Importantly, a recent study examining the whole-brain projection of 264 oxytocin neurons in the mouse paraventricular hypothalamic nucleus identified distinct neuron types with markedly different axonal projection patterns[23]. This discovery highlights the potential projection diversity within hypothalamic peptidergic neuron populations, which warrants further investigation.

In the present study, we employed fluorescence micro-optical sectioning tomography (fMOST)[23–25] and reconstructed the single-cell projectomes of over 7,000 hypothalamic neurons expressing specific neuropeptide genes, yielding, to our knowledge, the largest single-neuron projectome dataset for the hypothalamus. Analysis of this dataset identified two main classes and 31 projectome-defined neuron types with distinct axonal projection patterns, soma distribution and neuropeptide enrichments, accentuating the complexity of hypothalamic peptidergic axonal projections.

Results

Mapping single-cell projectomes of hypothalamic peptidergic neurons

To achieve bright, sparse and specific labeling of molecularly defined hypothalamic peptidergic neurons, we injected the hypothalamus with adeno-associated viruses (AAVs) carrying Cre-dependent green fluorescent protein (GFP) in genetically modified mice that expressed *Cre* recombinase under the control of a neuropeptide promoter. Alternatively, we injected AAVs that expressed GFP driven by an *Orexin* promotor in wild-type mice to label *Orexin*-expressing neurons (Fig. 1a, Extended Data Fig. 1, Supplementary Table 1 and Methods). After sufficient viral expression, brain samples were processed and imaged by fMOST (Fig. 1a), achieving 0.32 μm × 0.32 μm × 1 μm spatial resolution for the whole brain. To trace the axons of individually labeled axons, we employed a streamlined semi-automatic procedure with multiple rounds of quality control and cross-personal validation to ensure the precision and reliability of the traced results, as described previously[23,25,26] (Supplementary Fig. 1a and Methods). We then registered all traced projections onto the Allen Mouse Brain Common Coordinate Framework (CCFv3)[27] (Supplementary Fig. 1b; see Supplementary Table 2 for brain structure abbreviations) to permit cross-sample comparison. In total, we reconstructed the brain-wide projectome of 7,180 individual neurons from 16 peptidergic populations in 166 adult male mice, with their somata registered to the hypothalamus in the CCFv3 atlas (Fig. 1a,b and Supplementary Table 1).

Notably, the soma distribution of the neurons that we reconstructed closely corresponded to the known expression patterns of these neuropeptides[28] (Extended Data Fig. 2a). Specifically, for neurons marked by neuropeptides with localized expression (*Agrp*, *Avp*, *Crh*, *Orexin*, *Oxt*, *Pmch*, *Pomc* and *Vip*), 1,106 neurons (15.4% of the total 7,180) were obtained, and their somata were confined to hypothalamic regions corresponding to the expression of these neuropeptides. Most neurons (6,074 out of 7,180, 84.6%) were marked by broadly expressed neuropeptides (*Adcyap1*, *Nts*, *Penk*, *Pdyn*, *Sst*, *Tac1*, *Tac2* and *Trh*), and we found that their somata were also broadly distributed in the hypothalamus. Moreover, examining the published single-cell transcriptome data[22] provided further insights into the transcriptional diversity of these hypothalamic peptidergic neuron populations (Extended Data Fig. 3). This analysis revealed that these 16 neuropeptides were enriched in 368 out of the 1,451 (~25.4%) transcriptome-defined neuronal subtypes identified in the hypothalamus, encompassing both excitatory and inhibitory subtypes. Moreover, most (306 out of 368, 83.2%) of the subtypes were enriched for only one of the 16 neuropeptides, highlighting the specificity of neuropeptide expression patterns within the hypothalamus.

The somata of the reconstructed neurons occupied nearly all hypothalamic nuclei to varying degrees (Extended Data Fig. 2b). Approximately 15% of somata were located in the nebulous region, referred to as HY (hypothalamus) in the Allen Brain Atlas, supporting comprehensive hypothalamic coverage of the dataset. The axon arbors of these 7,180 neurons extended to occupy approximately 21.8% and 10.2% of the voxels (voxel size, 25 μm × 25 μm × 25 μm) on the ipsilateral and contralateral sides of the brain, respectively (Fig. 1c), indicating extensive brain-wide projections. Thus, we mapped, to our knowledge, the largest single-neuron projectome dataset for hypothalamic neurons expressing distinct neuropeptides. These projectome data are accessible at https://mouse.digital-brain.cn/projectome/hy.

Classification of hypothalamic peptidergic neurons based on single-cell projectomes

We first asked whether canonical projectome types exist in the hypothalamus, independent of soma location or neuropeptide expression. To this end, we tried to classify reconstructed hypothalamic peptidergic neurons based solely on their morphology. Manual inspection revealed that these neurons had limited dendritic structures but highly variable axon arborization (Fig. 1d), with only a small fraction (~9%) displaying seemingly stereotyped axon projection patterns. This variability was reflected in greater variance in the total axon length, axon branch numbers and target brain areas for hypothalamic peptidergic neurons compared to cortical or hippocampal neurons (Supplementary Fig. 2).

Fig. 1 | Single-cell projectomes of hypothalamic peptidergic neurons. a, The labeling and imaging procedure. We sparsely labeled hypothalamic neurons expressing 1 of the 16 indicated neuropeptides (left, bottom) and imaged the brain sample on an fMOST platform (right). The fluorescent image shows the axon processes of a labeled neuron. Scale bar, 50 μm. **b**, Soma distribution of the 7,180 reconstructed peptidergic neurons in various hypothalamic nuclei (color-coded) in 3D view with the three axes indicated on the side. See Supplementary Table 2 for nomenclature details. The somata of all neurons were mirrored to the same hemisphere of the brain. **c**, Axon projections of all 7,180 reconstructed neurons throughout the brain, with each axon labeled with a different color. **d**, Examples of the reconstructed neuron morphology in a whole-brain view. The expressed neuropeptide and the soma location of the neuron are indicated above the brain. The colors represent different neuronal components: red for soma, black for the axon and blue for dendrites. **e**, The algorithm for calculating the similarity score between neuron pairs. In brief, for each point in neuron A, we calculated the closest distance to points in neuron B, defined as $d(A_i)$, as shown on the left. For all points in neuron A, we calculated a mean and maximum value of all $d(A_i)$ values. We weighted these mean and maximum values by the portion of points in neuron A that had a $d(A_i)$ value below or above the mean and defined this as the directional A → B distance. The distance between the A–B neuron pair was the average of the two directional (A → B and B → A) distances. **f**, Summary of neuropeptide information (gene), soma location (location) and axon projections for the 7,180 reconstructed neurons clustered into the 31 projectome-defined types, labeled 1–31. Each tick represents the value of the total axon projection length (in μm) in each brain area marked on the left (in rows) with the scale shown above. We divided these types into two major classes: non-midbrain-projecting, highlighted in blue, and midbrain-projecting, of which types 16–22, highlighted in pink, represent the medulla and midbrain-projecting types; the rest, types 23–31, are highlighted in green. AHN, anterior hypothalamic nucleus; TU, tuberal nucleus; TMv, tuberomammillary nucleus, ventral part; MM, medial mammillary nucleus; DR, dorsal nucleus raphe; MY, medulla; IO, inferior olivary complex; NTS, nucleus of the solitary tract; PARN, parvicellular reticular nucleus; IRN, intermediate reticular nucleus; PB, parabrachial nucleus; PRNr, pontine reticular nucleus; PCG, pontine central gray; PA, posterior amygdalar nucleus; BMA, basomedial amygdalar nucleus; BLA, basolateral amygdalar nucleus; BST, bed nuclei of the stria terminalis; SI, substantia innominata; LS, lateral septal nucleus; ACB, nucleus accumbens; PT, parataenial nucleus; AM, anteromedial nucleus; SPFm, subparafascicular nucleus, magnocellular part; HPF, hippocampal formation; OLF, olfactory areas; CTXpl, cortical plate; STR, striatum; PAL, pallidum; CTXsp, cortical subplate.

https://doi.org/10.1038/s41593-025-01919-0

After exploring several methods[26,29,30], we adapted a method for categorizing complex dendritic tree structures[31] to classify the axon projection patterns of hypothalamic peptidergic neurons. Specifically, we calculated morphological similarity between neuron pairs by computing the weighted average of the closest distances for all traced points on these two neurons (Fig. 1e and Methods). Empirically, we found that this parameter of weighted average captured both partial and global morphological similarities between hypothalamic neuron pairs better than the mean or maximum value alone. Using the resulting similarity matrix, we employed agglomerative clustering with Ward's linkage to group neurons hierarchically into two main classes and 31 projectome-defined types (Fig. 1f and Supplementary Table 3). Class I (~40%, non-midbrain-projecting) includes types 1–15, and Class II (~60%, midbrain-projecting) includes types 16–31, with types 16–22 also projecting to the medulla. These 31 types represent the minimum number needed to preserve the approximately 9% of hypothalamic neurons with stereotype projections as distinct projectome-defined types (types 2, 4, 13, 20 and 22).

Axon projection patterns of the 31 projectome-defined types

Among neurons of types 1–15, grouped into the non-midbrain-projecting class (Class I), most displayed some targeting preferences for non-midbrain target areas outside of the hypothalamus, such as the cortex, pallidum, thalamus and striatum (Extended Data Fig. 4; see also Fig. 1f). For example, as shown in Extended Data Fig. 4a–f, type 1 and type 5 neurons exhibited strong projections to the central amygdalar nucleus (CEA) and the medial amygdalar nucleus (MEA); type 2 projected to the substantia nigra (SNr) and the external globus pallidus

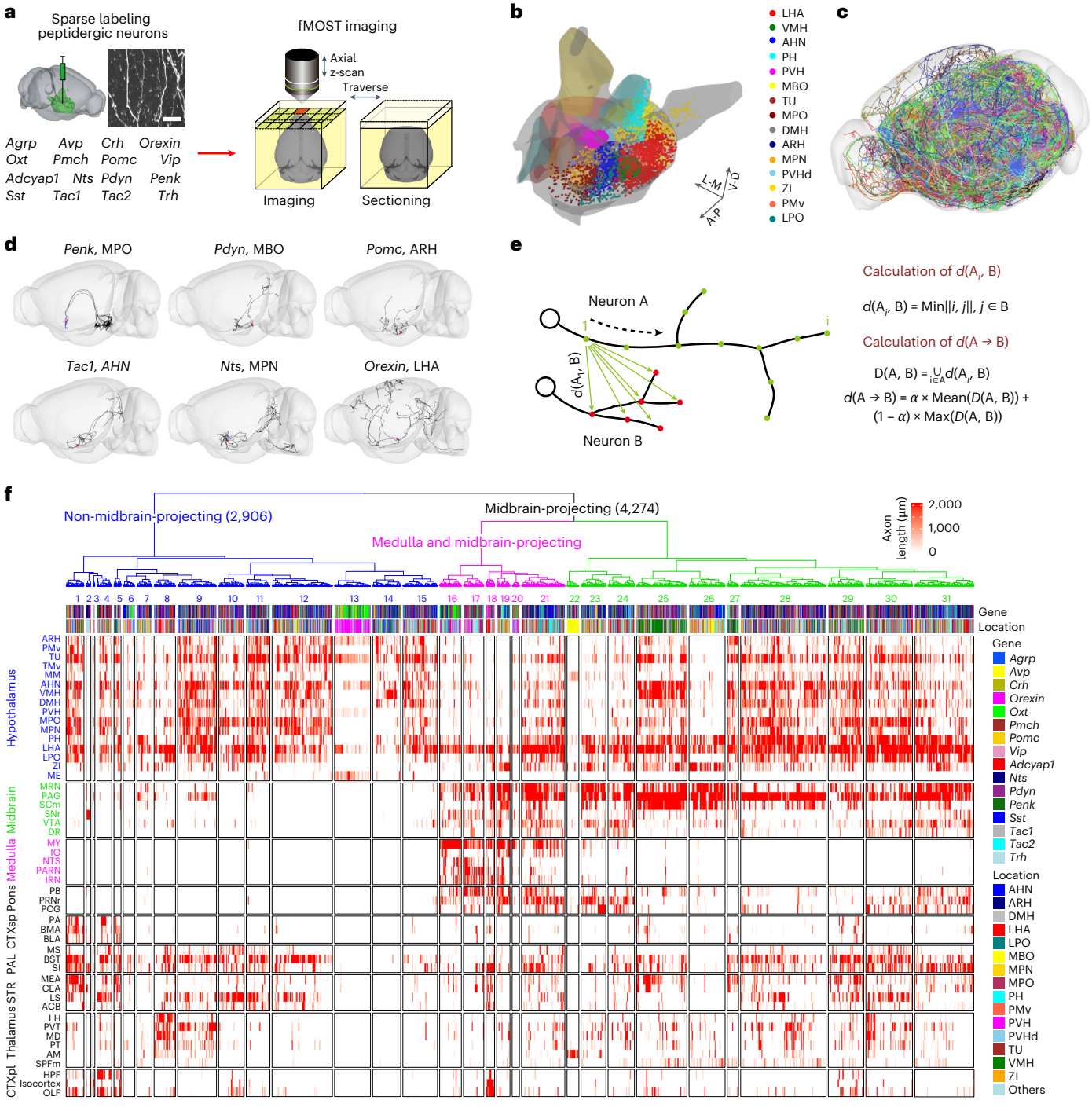

(GPe); type 3 projected to both the anterior cingulate area (ACA) and somatomotor (MO) areas; type 4 showed robust projections to CA1 of the hippocampus; and type 8 and type 9 projected to thalamic nuclei with differing preferences to the lateral habenula (LH), the mediodorsal nucleus of the thalamus (MD) and the paraventricular nucleus of the thalamus (PVT). Neurons in other types within Class I primarily terminated their axons within and around the hypothalamus, with types 6 and 7 projecting locally and types 10–15 extending projections to various hypothalamic nuclei involved in regulating innate behaviors (Extended Data Fig. 4g–j). Notably, type 13 exhibited restricted projections to the median eminence (ME) and the arcuate hypothalamic nucleus (ARH), confirming a previously known type of hypothalamic neurons projecting to the neurohypophysis[32,33] (Extended Data Fig. 4i).

By comparison, as shown in Extended Data Fig. 5, types 16–31 in the midbrain-projecting Class II projected with varying strengths to the periaqueductal gray (PAG) and also extended their axons to the ventral tegmental area (VTA) and the motor-related region of the superior colliculus (SCm) in the midbrain (Extended Data Fig. 5a). These types varied in their specific targeting preferences within the VTA, SCm, diverse hypothalamic nuclei (Extended Data Fig. 5a,g,h) and distinct PAG subdomains encompassing the anterior PAG (aPAG), rostral nuclei (interstitial nucleus of Cajal (INC), supraoculomotor periaqueductal gray (Su3), nucleus of Darkschewitsch (ND) and precommissural nucleus (PRC)) and longitudinally organized PAG columns (Extended Data Fig. 5j–l). Interestingly, bilateral PAG-projecting neurons targeted similar PAG columns/nuclei between the two hemispheres (Extended Data Fig. 5m), indicating a structural basis for bilateral control of PAG function by a single hypothalamic axon. Outside of the midbrain, types 16–22 further showed strong projections to pons and medulla, whereas types 23–31 exhibited limited projections to the medulla but did project to the pons (Extended Data Fig. 5a). For additional details on the projection patterns of neurons from types 16–31, see Supplementary Note.

We observed similar axon projection patterns across projectome-defined types when counting axon terminal numbers instead of total axon projection length (Supplementary Fig. 3), supported by a strong correlation between these two matrices in downstream brain regions (Supplementary Table 4). The emergence of target preferences among morphologically defined neuron types in a highly diverse dataset validates our classification approach.

To further corroborate the 31 projectome-defined types, we analyzed the MouseLight dataset[34], which contains the single-cell projectomes of 1,000 pan-neuronally labeled neurons, including 77 hypothalamic neurons. By calculating the similarity score of these 77 hypothalamic neurons to neurons in our dataset, we found alignment with 20 out of 31 identified projectome types (Supplementary Fig. 4 and Supplementary Table 5). Notably, all mammillary body (MBO) neurons in the MouseLight dataset displayed a stereotyped bifurcating axon projection pattern and were correctly categorized as type 22 neurons, consistent with our dataset (Supplementary Fig. 4). These results demonstrate that projectome-defined neuron types can be validated across datasets using different labeling and imaging techniques, highlighting the robustness and broad applicability of our classification result. In conclusion, we identified 31 distinct types, many with extensive axon collaterals. The Python library for neuron feature calculation and classification is available at https://pypi.org/project/pyswcloader/.

Skewed soma distribution and peptide enrichment in midbrain-projecting neurons

The cell-type-specific labeling method and the expanded hypothalamic coverage in our dataset (a 100-fold increase, 7,180 neurons compared to 77) enabled us to investigate the relationship among hypothalamic axon projection patterns, soma location and neuropeptide expression. A clear regional bias in soma distribution was evident for midbrain-projecting (Class II) neurons. By comparing the proportion of neurons in specific hypothalamic nuclei categorized as Class II to that in all other hypothalamic nuclei (excluding the one being examined), we found that Class II neurons were enriched in the lateral hypothalamic area (LHA) and the ventromedial hypothalamic (VMH) nucleus while being underrepresented in the paraventricular hypothalamic nucleus (PVH) and the ARH (Fig. 2a). When focusing on neurons expressing broadly distributed neuropeptides to minimize sampling bias, we further found that the VMH showed the highest density of Class II neurons, measured by neuron count per volume (Fig. 2a).

Among the peptidergic populations sampled within the VMH, Class II neurons were significantly enriched for the *Pdyn*, *Tac1*, *Adcyap1* and *Tac2* but not the *Sst* or *Penk* population (Fig. 2b). In contrast, the *Pdyn* and *Tac2*–expressing population in the nearby dorsal medial hypothalamic (DMH) nucleus showed an opposite enrichment for Class I neurons (% Class I: DMH *Pdyn* neurons, 72%, $P < 0.0001$; DMH *Tac2* neurons, 60%, $P = 0.0059$). These results reveal skewed soma distribution among midbrain-projecting hypothalamic neurons, with additional specificity observed in distinct peptidergic populations within the same nucleus.

To independently verify these findings, we injected retroAAVs encoding nuclearized GFP (mNeoGreen) into the midbrain (Fig. 2c and Methods) and observed robust retrograde labeling in the VMH (Fig. 2c). Subsequent sequential in situ hybridization analysis of VMH neurons using expansion-assisted iterative fluorescence in situ hybridization (EASI-FISH)[35,36] for the expression of several neuropeptides (Fig. 2d) further demonstrated significant enrichment of *Pdyn*, *Adcyap1* and *Tac2* in VMH GFP$^+$ neurons, with the most significant enrichment observed for neurons co-expressing *Pdyn* and *Adcyap1* (Fig. 2e,f). In contrast, a pattern of avoidance was observed for *Sst* expression in VMH GFP$^+$ neurons (Fig. 2e,f). These results independently validate our findings from the single-neuron projectome dataset and provide further support for selective peptide enrichment among midbrain-projecting VMH neurons.

Skewed soma distribution and peptide enrichment among projectome types

Next, we examined the relationship among projectome types, soma location and neuropeptide expression. First, most of the projectome types exhibited soma distribution skewed toward one or multiple hypothalamic nuclei. This resulted in a varied pattern of enrichments and occasional avoidance for multiple projectome types within most hypothalamic nuclei, with the LHA exhibiting a particularly complex pattern (Fig. 3a). Consequently, neuropeptides with restricted expression patterns, such as *Oxt*, *Orexin*, *Agrp* and *Pomc*, also demonstrated enrichments for projectome types whose soma distribution skewed toward the hypothalamic nuclei expressing these neuropeptides (Fig. 3a). Conversely, neuropeptides with broader expression displayed more complex enrichment and avoidance patterns across multiple projectome types and hypothalamic nuclei (Fig. 3a). As such, we uncovered some intricate relationships among axon projectome types, soma location and neuropeptide expression.

For example, *Oxt*, primarily labeling neurons in the PVH and its descending division (PVHd)[23], showed significant enrichment for projectome types 6, 13, 16 and 20. Not surprisingly, the soma of type 6 was preferentially distributed in PVHd, type 13 in PVH and types 16 and 20 in both PVH and PVHd (Fig. 3b–e). Interestingly, *Sst* neurons in the LHA and the zona incerta (ZI) were also enriched for type 6, whereas *Pdyn* neurons in the PVH and PVHd were enriched for type 20, indicating potential function convergence among different peptidergic populations. Similarly, *Orexin*, primarily labeling neurons in the LHA, showed enrichment for types 3 and 18, both with soma skewed toward the LHA and projecting to the isocortex (Fig. 3f,g), whereas type 3 also exhibited enrichment for the *Trh* population in the ZI. Concurrently, the LH-projecting type 8 neurons, also with skewed soma distribution in the LHA, displayed enrichment for *Adcyap1* but not for *Orexin* (Fig. 3h).

https://doi.org/10.1038/s41593-025-01919-0

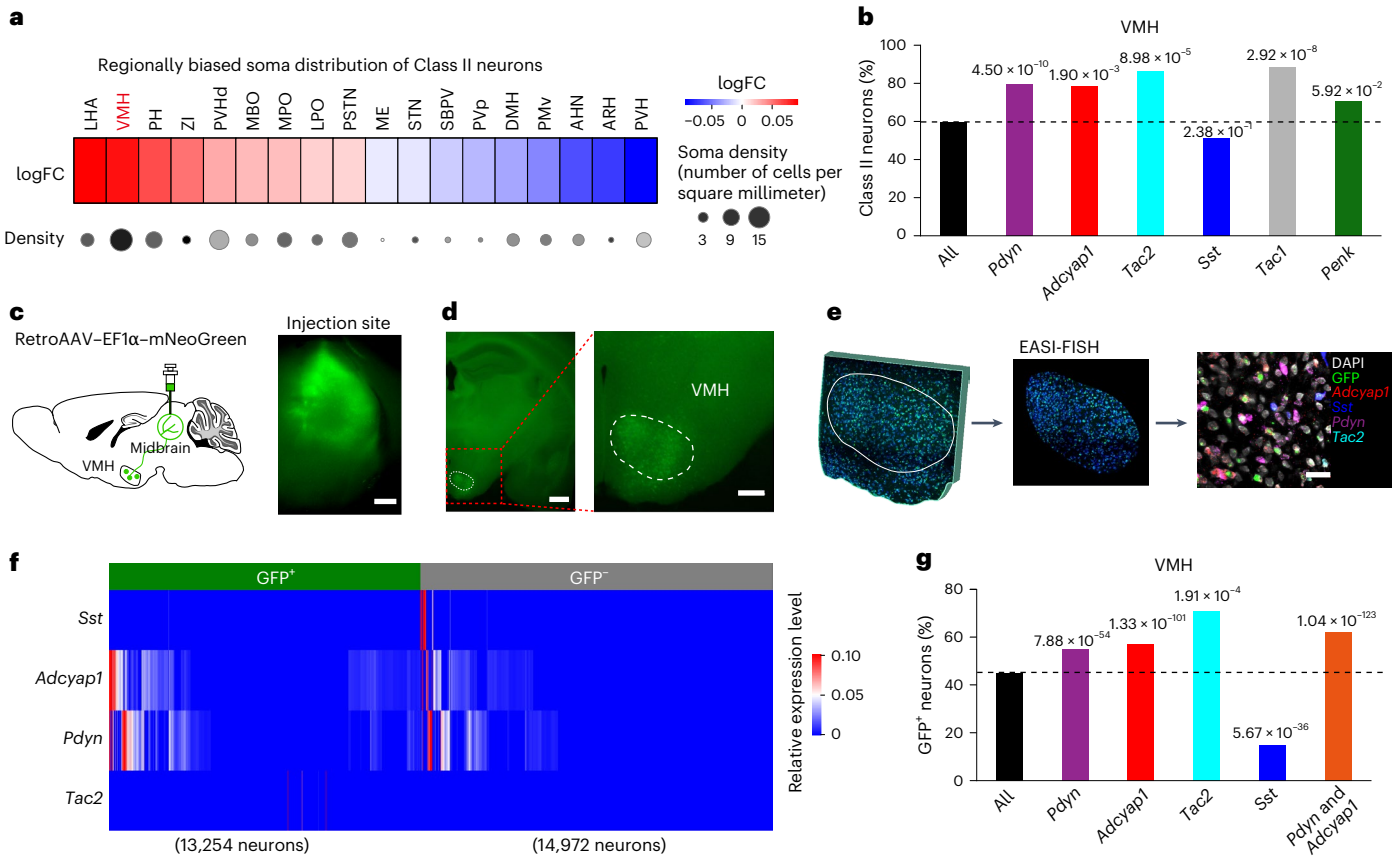

Fig. 2 | Skewed soma distribution and peptide enrichment in midbrain-projecting neurons. a, Regionally biased soma distribution of Class II (midbrain-projecting) neurons. The top heatmap shows the enrichment, represented by the $\log_2$ fold change (logFC) value, of the percentage of neurons in specific hypothalamic nuclei that fall into Class II, normalized by the percentage of Class II neurons in all other hypothalamic nuclei, excluding the one being examined. Only nuclei with statistically significant logFC values are displayed ($P < 0.05$). Below: the dot map illustrates the density of Class II neurons in each nucleus, focusing on those expressing the broadly distributed neuropeptide (*Adcyap1*, *Nts*, *Pdyn*, *Penk*, *Sst*, *Tac1*, *Tac2* and *Trh*). The dot size reflects the neuron density, and the grayscale filling indicates the average axon projection length of these neurons within each hypothalamic nucleus. PVp, periventricular hypothalamic nucleus, posterior part; SBPV, subparaventricular zone. **b**, The percentage of VMH neurons classified as Class II within each indicated neuropeptide population. The values above each bar represent the *P* values calculated using a two-tailed Fisher's exact test with Benjamini–Hochberg correction, comparing the percentage of Class II neurons in each neuropeptide population to the overall dataset percentage (4,274 out of 7,180, ~59.5%). VMH Class II neurons were significantly enriched in *Pdyn*, *Tac1*, *Adcyap1* and *Tac2* populations but not in the *Sst* or *Penk* population. **c**,**d**, Injection of retroAAV encoding mNeoGreen, a version of GFP, into the midbrain (**c**) resulted in intense labeling in the VMH (**d**). Scale bars, 500 µm for **c** and **d** (left) and 200 µm for **d** (right). **e**, The experimental procedure of EASI-FISH for in situ detection of neuropeptide expression and GFP signals in the VMH. **f**, Heatmap representation illustrating the relative expression levels of the indicated neuropeptide in each GFP$^+$ and GFP$^-$ neuron in the VMH. The number in the parentheses indicates the total number of neurons analyzed from two adult male animals. **g**, The percentage of neurons in each indicated VMH neuropeptide population that are also GFP$^+$, as shown in **f**. The values above each bar represent the *P* values calculated using a two-tailed Fisher's exact test with Benjamini–Hochberg correction, comparing the percentage of GFP$^+$ neurons in each neuropeptide population to the overall dataset percentage. GFP$^+$ VMH midbrain-projecting neurons are enriched in the *Pdyn*, *Adcyap1* and *Tac2* populations, including those co-expressing *Pdyn* and *Adcyap1*, but not in *Sst* neurons.

In addition, the intra-hypothalamic-projecting types 10 and 15, lacking noticeable skewness in soma location, displayed enrichment for *Adycap1* and *Sst*, respectively (Fig. 3a,i). On the other hand, the bilaterally PAG-projecting type 25, broadly dispersed with some biased soma locations in the VMH, displayed enrichment for *Tac1* (Fig. 3j), and type 30, favoring the ipsilateral PAG, showed biased soma distribution in the medial preoptic (MPO) area and enrichment for *Nts* (Fig. 3k). Together, these examples illustrate the complex relationships among axon projectome types, soma location and neuropeptide expression.

Given the comprehensive coverage of major hypothalamic nuclei and the sampling depth of neuropeptides, particularly those with broad distribution (Extended Data Figs. 2 and 3), the observed selectivity in biased soma distribution and distinct neuropeptide enrichment patterns among specific projectome types cannot be explained solely by sampling bias. Instead, these findings suggest that the interplay among axon projection patterns, soma location and neuropeptide expression represents inherent characteristics of defined neuronal populations. Consequently, integrating projectome-defined types with molecular markers and soma location should provide a deeper understanding of the specific neuronal types involved in distinct hypothalamic functions.

Topographic organization of hypothalamic peptidergic projections

To further investigate the interplay among axon projection patterns, soma location and neuropeptide expression and to glean insights into the potential functions of hypothalamic peptidergic neurons by integrating single-neuron projectome data, we conducted an in-depth analysis of specific peptidergic neurons within projectome types (2, 4, 13, 20 and 22) that exhibited distinct morphological and projection characteristics (Figs. 3c,e, 4a,e,h and 5b,c and Extended Data Fig. 4c,d,i). Notably, types 13 and 20, enriched for PVH *Oxt* neurons (Fig. 3), displayed simple and typically unbranched axon projections

https://doi.org/10.1038/s41593-025-01919-0

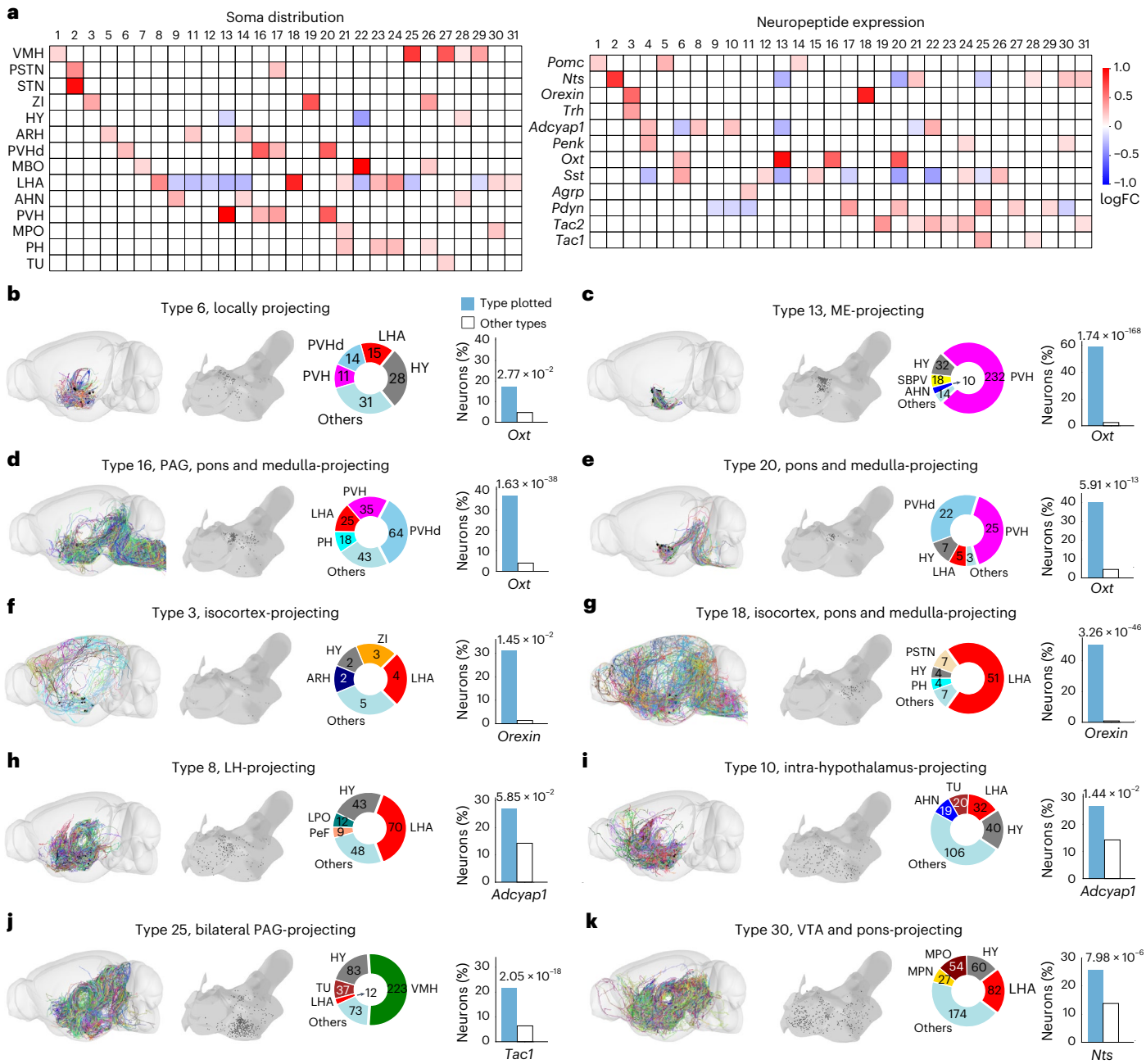

Fig. 3 | Skewed soma distribution and peptide enrichment in projectome types. a, Heatmap representation illustrating the enrichment or avoidance of soma distribution (left) and neuropeptide populations (right) across distinct projectome types (columns) for various hypothalamic nuclei or neuropeptide populations (rows). Only $\log_2$ fold change (logFC) values that meet the significance threshold ($P < 0.05$, two-tailed Wilcoxon rank-sum test with Bonferroni correction) are shown. **b**–**k**, Examples of projectome-defined types (6 (**b**), 13 (**c**), 16 (**d**), 20 (**e**), 3 (**f**), 18 (**g**), 8 (**h**), 10 (**i**), 25 (**j**) and 30 (**k**)) exhibiting enrichment for specific neuropeptide populations. For each projectome type shown in the panels, the figures (from left to right) include the combined axon projections of neurons visualized in a 3D brain representation, the distribution of soma within the hypothalamus, neuron counts within each designated hypothalamic nucleus/region and the percentage of neurons in the indicated projectome type (blue bar) versus all other types (white bar) that express the specified neuropeptide. Statistical significance was determined using a two-tailed Fisher's exact test with Benjamini–Hochberg correction, with the exact P values for **b**–**k** indicated above the corresponding bar graphs. PeF, perifornical nucleus.

targeting the ME and the brainstem, respectively (Fig. 3c,e), representing specialized hypothalamic neurons for the release of oxytocin into the posterior pituitary or exerting descending control over brainstem and spinal cord functions.

Type 2 neurons showed skewed soma distribution to the subthalamic nucleus (STN) and the para-subthalamic nucleus (PSTN) and were enriched for *Nts* expression (Fig. 3a). We found that the somata of *Nts*-expressing type 2 neurons formed a slanted strip across the STN and PSTN (Fig. 4a,b). In addition, these neurons exhibited bifurcating axon collaterals, projecting anteriorly to the GPe and posteriorly to the SNr (Fig. 4a), two crucial components of the basal ganglia circuit governing motor function[37]. Strikingly, the projections from *Nts*-expressing type 2 neurons to the GPe and SNr displayed a pronounced topographic organization along the medial-lateral (M-L) axis (Fig. 4c). Topography along the dorso-ventral (D-V) axis was also evident, albeit in opposite orientations for projections in the SNr and GPe (Fig. 4d). Despite

previous studies examining STN projections[38,39], topographic arrangements of individual axon collaterals in both SNr and GPe had never been reported, highlighting the power of the single-neuron projectome analysis. As single-cell RNA sequencing (scRNA-seq) analysis identified *Nts*-expressing neurons as a transcriptionally distinct population in the STN[40], type 2 *Nts*-expressing neurons thus represent a unique category of transcriptionally defined, projectome-defined and regionally confined neurons that project topographically to two key brain regions in the basal ganglia circuit, suggesting a specialized role in motor control.

In addition, type 4 exhibited enrichment for *Penk* and *Adycap1* (Fig. 3a). *Penk*-expressing type 4 neurons, projecting to the dorsal CA1 in a stereotyped manner (Fig. 4e), were primarily located in the MPO and HY regions of the hypothalamus but also dispersed into neighboring areas, such as the medial septum (MS) and the nucleus of the diagonal band (NDB), in a continuous strip (Fig. 4f). Consequently, these adjacent *Penk*-expressing neurons around the hypothalamus were included into our analysis. Notably, the soma distribution of these *Penk*-expressing neurons along the D-V axis showed a distinct topographical correspondence with their terminals in the dorsal CA1 along the anterior-posterior (A-P) axis (Fig. 4g). This topographic correspondence was not observed for nearby non-*Penk* neurons that also projected to dorsal CA1 (Extended Data Fig. 6a), implying a specialized function involving *Penk* signaling within this hypothalamic-hippocampal pathway. On the other hand, *Adcyap1*-expressing type 4 neurons, with soma dispersed across multiple hypothalamic nuclei, predominantly projected to the ventral CA1 with a notable topography between their termini along the M-L axis in CA1 and their somata distribution along the D-V axis in the hypothalamus (Extended Data Fig. 6b,c). These findings indicate hypothalamic regulation of dorsal and ventral CA1 regions via distinct peptidergic populations within the same projectome type (4), aligning with the established functional division between dorsal and ventral CA1 (ref. 41).

Finally, we examined the axon organization of MBO type 22 neurons (Fig. 4h). Previous studies indicated that neurons residing within the medial and lateral divisions of the MBO targeted specific subregions within the anterior thalamic nuclei (ATN) to convey distinct information[42,43]. Leveraging the single-axon resolution of our dataset, we uncovered an exceptionally intricate topographic organization in MBO projections to the ATN that spanned all three axes (A-P, D-V and M-L) (Fig. 4i,j and Extended Data Fig. 7a), surpassing the previously proposed simple topological correspondence within a single axis[43]. Further analysis revealed unique axon projection patterns and topographic organization within the ATN for each MBO peptide population (Fig. 4k–n). For *Tac2*-expressing type 22 neurons, primarily located in the lateral MBO, a topographic correspondence of axon distribution along the D-V axis in ATN with the soma distribution along the M-L axis was observed (Fig. 4l and Extended Data Fig. 7c). In contrast, such a topographic correspondence was not observed in *Nts*-expressing type 22 neurons, predominantly found in the medial MBO (Fig. 4n and Extended Data Fig. 7c). These findings suggest a nuanced interplay between neuropeptide expression and topographic organization within the MBO–ATN circuitry, warranting further functional investigation. A topographic organization was notably absent in the bifurcated axon collaterals of type 22 neurons targeting the midbrain and pons (Extended Data Fig. 7b), emphasizing the pathway-specific nature of this organization.

Thus, our analysis unraveled topographical arrangements of axon projections originating from distinct neuropeptide populations targeting specific downstream areas. Topography within the connectome plays a crucial role in sensory mapping and higher cognitive function[44,45]. Our findings, therefore, suggest the potential unique contributions of these hypothalamic peptidergic populations to processes such as motor control, learning and memory. Moreover, a preliminary examination of other projectome types hints at possible topographical arrangements in additional brain regions (Supplementary Fig. 5), indicating a vast unexplored territory in understanding hypothalamic projections. These examples demonstrate that incorporating single-neuron projectome data into the existing framework of hypothalamic neuron types holds promise for uncovering novel insights into hypothalamic neural connectivity underlying distinct functions.

Analyzing the single-cell projectome of key hypothalamic neuropeptide populations

In the preceding analysis (Figs. 1–4), we identified two main classes and 31 projectome-defined types among 7,180 hypothalamic neurons expressing distinct neuropeptides (Fig. 1). These projectome types exhibit regionally biased soma distribution and distinct neuropeptide enrichment (Figs. 2 and 3), consistent with bulk anterograde tracing results (https://connectivity.brain-map.org/) that show regionally organized hypothalamic projections. Many projectome types also display target selectivity and preferences, with some showing topographic innervation of distinct downstream regions (Fig. 4), highlighting the power of single-neuron projectome analysis. Additionally, the presence of multiple neuropeptide-expressing populations within the same projectome types suggests functional convergence among hypothalamic neurons expressing different neuropeptides.

Although the above analyses provide an overview of the axon projection organization of hypothalamic neuropeptide populations, the function of these projectome-defined types remains unclear and requires further analysis. Thus, a complementary approach would be to use single-neuron projectome analysis to identify distinct projectome types within defined hypothalamic neuropeptide populations of known important functions, which may elucidate the structural basis of functional divergence within the same neuropeptide population. For instance, analyzing the whole-brain projection of oxytocin neurons identified distinct subpopulations with markedly different axonal projection patterns[23]. To facilitate such analyses, our publicly accessible website (https://mouse.digital-brain.cn/projectome/hy) offers a platform where registered users can explore, visualize and download data to perform various focused analyses on neurons of interest. Here we highlight several standard analyses using *Orexin*-expressing, *Agrp*-expressing and *Pomc*-expressing neurons as examples (Figs. 5 and 6). The computer code used for feature calculation in these analyses is available as a Python library at https://pypi.org/project/pyswcloader/.

LHA *Orexin*-expressing neurons. *Orexin*-expressing neurons in the LHA and nearby areas, known for their complex regulatory roles in behaviors[46], are recognized as one single transcriptionally defined type of hypothalamic excitatory neurons through scRNA-seq and multiplexed error-robust fluorescence in situ hybridization (MERFISH) analysis[21] (Extended Data Figs. 3 and 8a and Methods). Previous bulk tracing studies identified that *Orexin* neurons project via four routes, including ventral and dorsal and ascending and descending pathways[15] (Fig. 5a). However, the specific path preferences and targeting patterns of individual axons remained unclear. Our initial grouped analysis revealed that, among all reconstructed hypothalamic neurons, *Orexin*-expressing neurons were significantly enriched for type 3, cortex-projecting, non-midbrain-projecting neurons, and type 18, midbrain-projecting neurons also targeting the pons, medulla and cortex (Fig. 3f,g). These findings strongly indicate the presence of distinct projectome types within *Orexin*-expressing neurons.

To this end, we examined the projection patterns of all 102 *Orexin*-expressing neurons in our dataset in more depth, first confirming their primary somatic localization in the LHA (Fig. 5b). Collectively, their axon projections spanned the entire brain, targeting all major structures identified at the population level (Fig. 5c,d). Individual axons exhibited considerable morphological and target variation (Fig. 5e). Using morphology-based clustering analysis, we identified five projectome-defined types labeled ‘α’ through ‘ε’ (Fig. 5e). The soma distribution of these types was intermingled (Fig. 5f). However,

https://doi.org/10.1038/s41593-025-01919-0

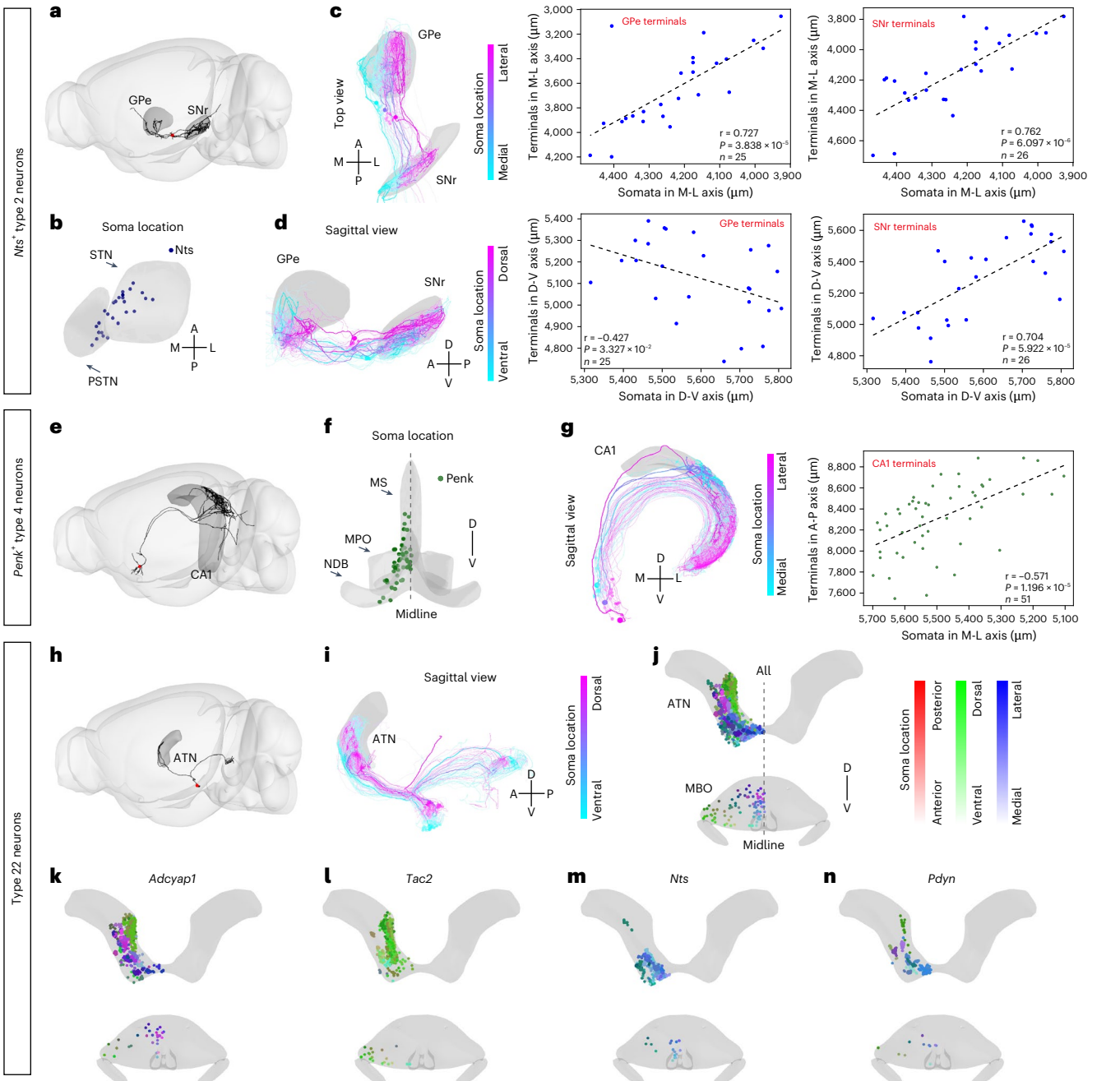

Fig. 4 | Topographic arrangement of hypothalamic peptidergic neuronal projections. a–**d**, Topographic organization of axon projections from *Nts*-expressing (*Nts*$^+$) type 2 neurons. **a**, Morphology of an individual *Nts*$^+$ type 2 neuron displaying bifurcating axon collaterals targeting GPe and SNr. **b**, Schematic illustrating the soma location of *Nts*$^+$ type 2 neurons in the STN and PSTN. Each dot indicates a neuron. Axes are indicated on the side. **c**,**d**, The topographic organization of axon projections of *Nts*$^+$ type 2 neurons along the M-L axis (**c**) and the D-V axis (**d**) in GPe and SNr. Examples of the morphology of a pair of neurons are shown on the left. Shown on the right is a linear regression analysis examining the relationship between the soma position (*x*) and the center position of projections in downstream targets (*y*) along the specified axes. Each dot represents data from a single neuron. The '*r*' values indicate the regression coefficient, and the *P* values were calculated using a two-tailed *t*-test. **e**–**g**, Topographic organization of axon projections from *Penk*-expressing (*Penk*$^+$) CA1-projecting (type 4) neurons. **e**, Morphology of an individual *Penk*$^+$ type 4 neuron displaying projections to CA1. **f**, Schematic illustrating the soma location of *Penk*$^+$ type 4 neurons in the MPO and other *Penk*$^+$ neurons in the MS and the NDB. **g**, The topographic organization of axon projections of *Penk*$^+$ neurons along the A-P axis in CA1 corresponds to the M-L axis of the soma distribution. Examples of the morphology of a pair of neurons are shown on the left, and a linear regression analysis examining the relationship between the soma position (*x*) and the center position of projections in downstream targets (*y*) along the specified axes is shown on the right. Each dot represents data from a single neuron. The '*r*' values indicate the regression coefficient, and the *P* values were calculated using a two-tailed *t*-test. **h**–**n**, Topographic organization of axon projections from MBO type 22 neurons. **h**, Morphology of an individual MBO type 22 neuron displaying bifurcating axon collaterals targeting ATN and midbrain/brainstem areas. **i**, Two example neurons illustrating the topographic organization of axon projections of MBO type 22 neurons in the ATN along the A-P axis show an inverse relationship with the D-V axis of the soma distribution. **j**, Representation of the overall topographic organization of axon projections from all MBO type 22 neurons in ATN relative to the soma location of these neurons along the three axes. **k**–**n**, The topographic organization of axon projections in ATN from type 22 MBO neurons expressing the indicated peptide (*Adcyap1* (**k**), *Tac2* (**l**), *Nts* (**m**), *Pdyn* (**n**)), relative to the soma location of these neurons along all three axes. In **j**–**n**, the soma location and axon projections of individuals are color-coded along the three axes using the scale shown in **j**.

https://doi.org/10.1038/s41593-025-01919-0

axon projections of each type displayed characteristic differences: 'α' preferred the ventral ascending pathway, 'δ' the ventral descending pathway and 'ε' the ventral and dorsal descending pathways, whereas 'β' and 'γ' used both ascending and descending routes (Fig. 5g–j and Extended Data Fig. 8b,c). As such, types 'β' and 'γ' strongly innervated the cortex and forebrain structures and encompassed most *Orexin* neurons previously classified as types 3 and 18 in the whole dataset (Fig. 5g), with 'γ' exhibiting the most extensive cortical arborizations and preferentially innervating visual (VIS) areas and the retrosplenial (RSP) area (Fig. 5h,i and Extended Data Fig. 8b). Consistently, correlation analysis of individual neuron projection strength further revealed coordinated targeting of cortical domains, such as RSP and VIS, by *Orexin* neurons (Extended Data Fig. 8d).

In addition, types 'δ' and 'ε' had limited cortical targets, with 'δ' projecting mainly via the ventral descending pathway to the medulla and 'ε' primarily targeting the PAG, SCm and pons via the dorsal descending pathway (Fig. 5f). Notably, type 'δ' exhibited simple, unbranched axon projections, potentially extending beyond our imaging limits to the spinal cord (Fig. 5h–j), suggesting a specialized type dedicated to spinal control and sensory processing. Thus, *Orexin* neurons comprise multiple projectome types with distinct axon innervation patterns, providing a structural basis for the diverse functions observed in these neurons.

ARH *Agrp*-expressing and *Pomc*-expressing neurons. Similarly, we compared the single-cell projectomes of *Agrp* and *Pomc* neurons in the ARH (Fig. 6a), which regulate feeding behaviors in opposing directions[47,48]. We sought to determine if there are differences in projection patterns between individual ARH *Agrp* and *Pomc* neurons, which could serve as an additional mechanism for their functional specialization besides releasing functionally antagonistic neuropeptides. A qualitative examination of axon projections of ARH *Agrp* ($n = 62$) and *Pomc* ($n = 129$) neurons highlighted that *Pomc*, but not *Agrp*, neurons displayed significant projections to the midbrain, pons and medulla regions (Fig. 6b). This difference was further quantified by higher percentages of neurons projecting and stronger projection strengths of individual *Pomc* neurons in areas such as the PAG, midbrain reticular nucleus (MRN), SCm and VTA (Fig. 6c,d). Notably, injecting retroAAVs[49] into the PAG labeled a higher percentage of *Pomc* neurons (Extended Data Fig. 9a,b), further confirming that more *Pomc* neurons project to the PAG, as shown by single-neuron projectome analysis. By comparison, individual *Agrp* neurons exhibited more robust projections to hypothalamic targets, including the PVH, PVHd, anteroventral periventricular nucleus (AVPV) and ME (Fig. 6d).

To further examine differences in projection patterns between *Agrp* and *Pomc* neurons, we used morphology-based clustering, revealing four types: 'M', 'L', 'A' and 'I'. These types displayed preferential projections to the Midbrain ('M'), Locally within ARH ('L'), medial and central Amygdala on the contralateral side ('A') and Intra-hypothalamically ('I'), respectively (Fig. 6e,f and Extended Data Fig. 9c). Consistent with the finding that more *Pomc* neurons project to the PAG, we observed a significant enrichment ($P = 0.035$) for 'M' type in the *Pomc* population (Fig. 6g). Additionally, we found that many *Agrp* neurons projected collaterally to multiple downstream targets (Extended Data Fig. 9d,e), challenging the previously proposed 'one-to-one' projection pattern inferred from retrograde labeling methods[50]. These results underscore the complex and divergent projection patterns of *Agrp* and *Pomc* neurons. In conclusion, these examples highlight the value of our dataset as a resource for exploring the projection patterns of specific hypothalamic neuron populations and offering insights into their functional diversity.

Distinct PAG subdomains revealed by coordinated hypothalamic neuron innervation

Furthermore, beyond providing a detailed depiction of the axon projections of individual hypothalamic peptidergic neurons, the extensive coverage of our dataset enabled an exploration of the mesoscale organizational principles underlying hypothalamic projections to downstream targets, with the PAG being a prominent recipient (Extended Data Fig. 10a).

Situated between the forebrain and lower brainstem/spinal cord structures, the PAG plays a crucial role in the top-down modulation of motor and autonomic function[51,52]. Although previous studies distinguished the rostral and caudal PAG, along with a columnar organization within the caudal PAG, our research revealed many types of PAG-projecting hypothalamic neurons that co-innervated multiple PAG columns, frequently pairing the ventrolateral PAG (vlPAG) with the lateral PAG (lPAG) and the dorsomedial PAG (dmPAG) with the dorsolateral PAG (dlPAG) (Extended Data Fig. 5j–n). These results suggest the co-regulation of PAG subdomains by single hypothalamic axons that transcend the previously defined nuclei or column boundaries. Remarkably, similar co-innervation of multiple PAG subdomains was reported in analyses of CEA neuron populations projecting to the PAG[53,54], indicating potential functional relevance.

To investigate this further, we subdivided the ipsilateral PAG into cubes of 100 μm × 100 μm × 100 μm in size each, allowing for a more detailed analysis of co-innervation patterns of PAG subdomains by hypothalamic axons. We then computed pairwise correlations among hypothalamic axon arbors within these cubes and conducted a clustering analysis based on the resulting correlation matrix (Fig. 7a). This analysis revealed seven distinct PAG subdomains, each demonstrating high inter-subdomain correlation in hypothalamic projections (Fig. 7b). These innervation-based PAG subdomains maintained the rostral-caudal and dorsal-ventral distinction as in the conventional PAG column/nuclei nomenclature (Fig. 7c). However, particularly noteworthy was the significant reconfiguration of part of the three longitudinal columns previously identified as dlPAG, lPAG and vlPAG into three innervation-based subdomains that showed a previously unrecognized A-P and M-L divide (Fig. 7b,c). Moreover, hypothalamic neurons from specific nuclei and expressing specific neuropeptide populations appeared to exhibit distinct preferences to target these

Fig. 5 | Multiple projectome types of *Orexin*-expressing neurons. a, Schematics depicting four axon projection pathways (color-coded) of *Orexin* neurons described in previous studies: the ventral ascending (red), dorsal ascending (green), ventral descending (blue) and dorsal descending (purple) pathways. AON, anterior olfactory nucleus; LC, locus ceruleus; MOB, main olfactory bulb; OT, olfactory tubercle; SC, superior colliculus; TM, tuberomammillary nucleus. **b**, The soma location of the 102 *Orexin* neurons is shown in a coronal section. **c**, Axon projections of the 102 *Orexin* neurons throughout the brain. **d**, Axon projection intensity of the 102 *Orexin* neurons in indicated brain areas. LDT, laterodorsal tegmental nucleus; TMd, tuberomammillary nucleus, dorsal part. **e**, Five projectome-defined types of *Orexin* neurons, termed 'α' through 'ε', were identified using morphology-based clustering analysis. Projections of a representative neuron (upper) and all neurons (lower) for each type are plotted. **f**, Soma location of the *Orexin* neurons for each projectome-defined type. **g**, Correspondence between *Orexin* projectome types and the 31 projectome types defined based on the entire dataset. **h**, Summary of axon projection length (in μm) for individual neurons of the five projectome-defined types in each brain area labeled on the left. Each tick represents the value of the axon projection length of a given neuron in a heatmap fashion with the scale shown above. PIR, piriform area; ENT, entorhinal area; ORB, orbital area; SS, somatosensory areas; GRN, gigantocellular reticular nucleus; PGRNl, paragigantocellular reticular nucleus, lateral part; IC, inferior colliculus; PPN, pedunculopontine nucleus. **i**,**j**, Violin plot of the projection length (in μm) of individual neurons in the five projectome-defined types in specific target areas along the ascending (**i**) or descending (**j**) pathways. Each circle represents an individual neuron.

https://doi.org/10.1038/s41593-025-01919-0

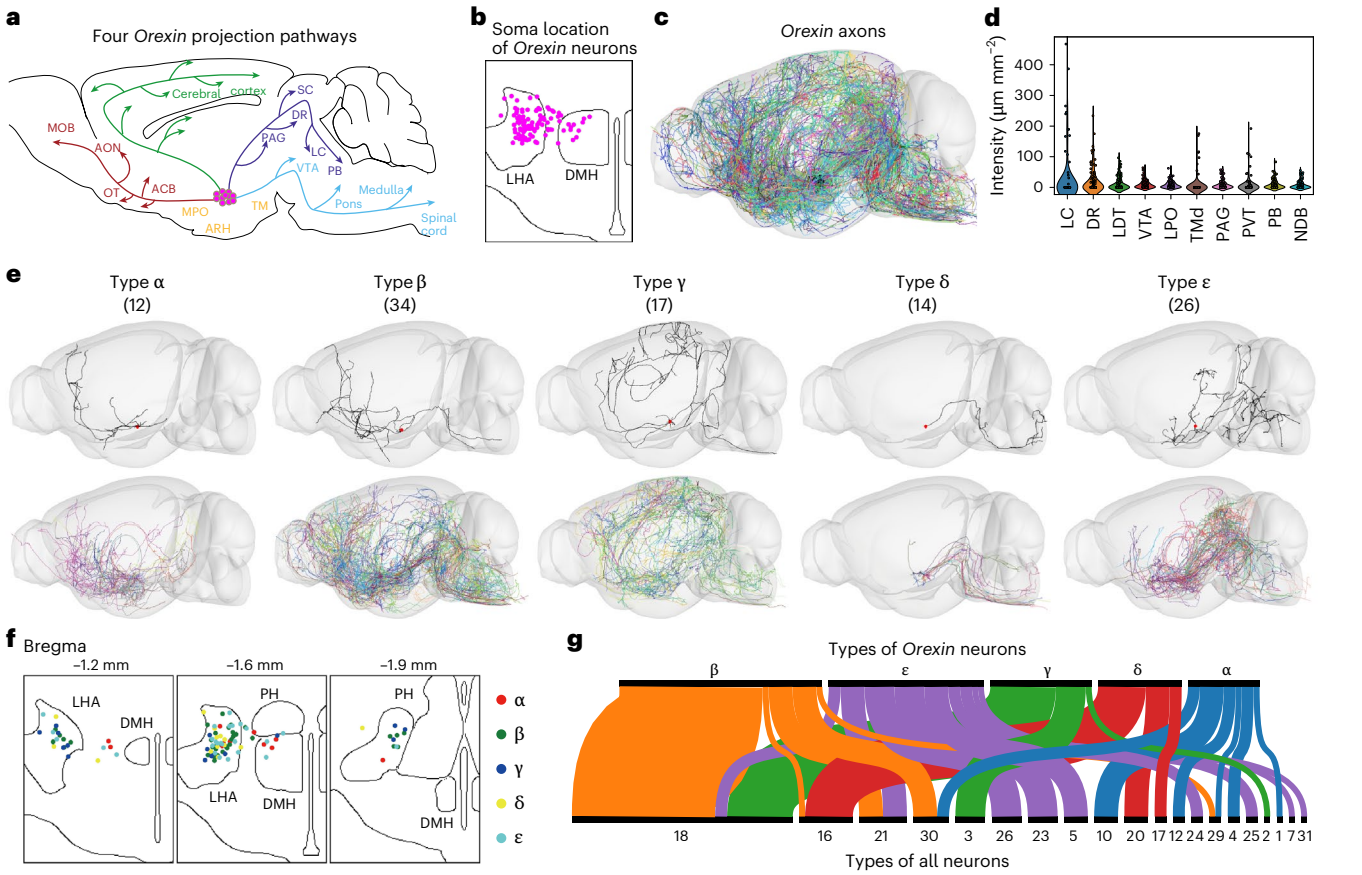

https://doi.org/10.1038/s41593-025-01919-0

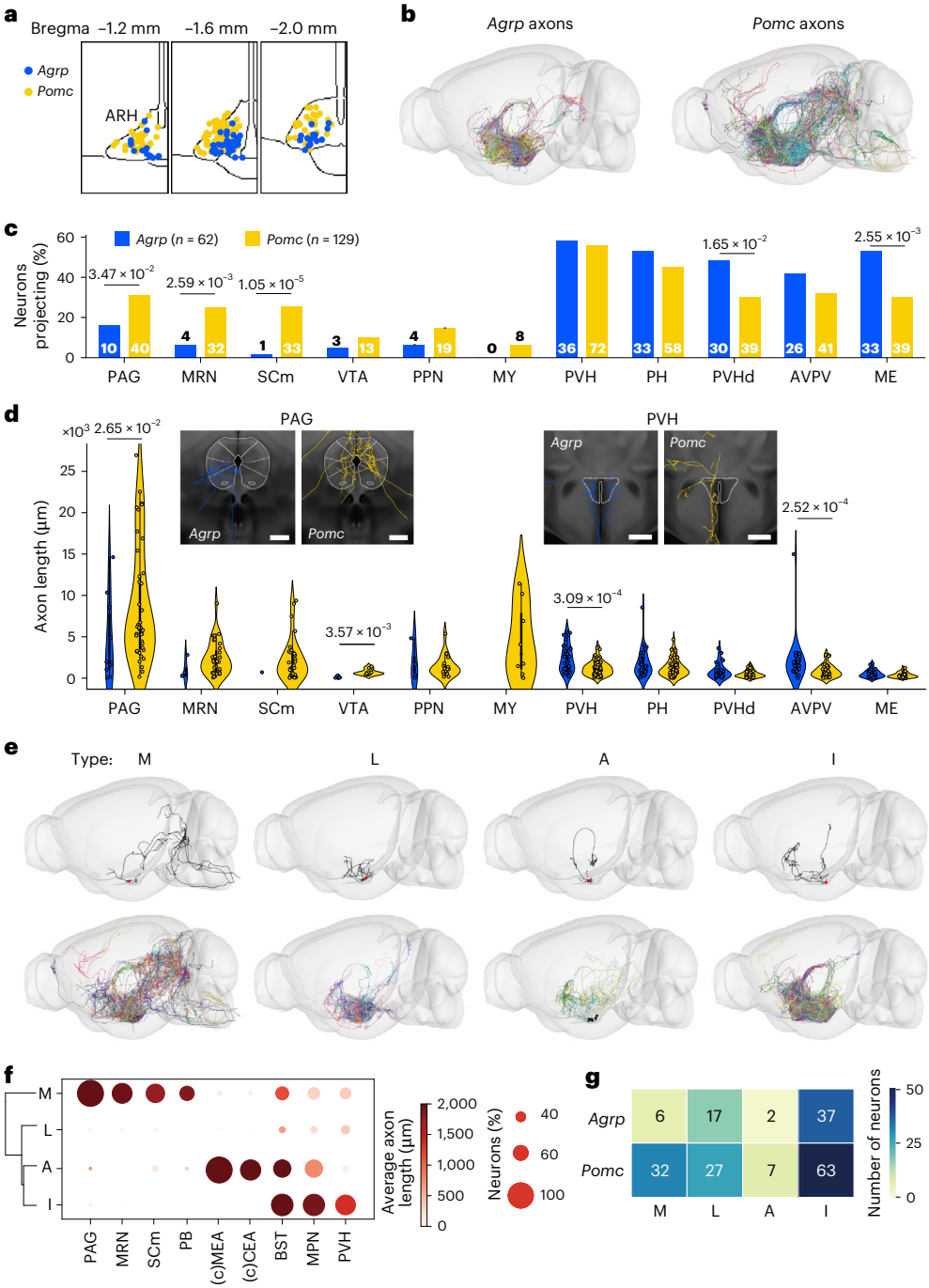

Fig. 6 | Arcuate *Agrp* and *Pomc* neurons differ in projectome types. a, Soma locations of the *Agrp* neurons (blue dots) and *Pomc* neurons (yellow dots) in the arcuate nucleus. **b**, Total axon projections of all *Agrp* (left) and *Pomc* (right) neurons throughout the brain. The projections of individual neurons are represented by different colors. **c**, Percentage of neurons projected to the indicated brain regions ($n = 62$ *Agrp* neurons (blue) and 129 *Pomc* neurons (yellow)). Exact counts of neurons projecting to each region are displayed inside or above the bars. Statistical significance (P value) was calculated using a two-tailed Fisher's exact test without correction for multiple comparisons and is shown above the bars for regions with $P < 0.05$. **d**, Axon projection lengths of individual neurons (represented as circles in the violin plot) projecting to the indicated brain regions. Exact neuron count for each region is the same as shown in **c**. In the box plots overlaid on the violin plot, the box represents the interquartile range (Q1–Q3), and the whiskers extend to the minimum and maximum values within Q1 − 1.5× interquartile range (IQR) and Q3 + 1.5× IQR. Statistical significance was assessed using a two-tailed Mann–Whitney U-test without corrections for multiple comparisons, with P values less than 0.05 indicated above the respective regions. Representative images show axon projections from an example *Agrp* or *Pomc* neuron in PAG or PVH. Scale bars, 500 μm. **e**, Morphology-based clustering analysis identified four projectome-defined types of *Agrp* and *Pomc* neurons, designated as 'M', 'L', 'A' and 'I'. 'M' refers to Midbrain-projecting neurons; 'L', neurons projecting Locally within ARH; 'A', neurons projecting to the medial and central Amygdala on the contralateral side; and 'I', neurons projecting Intra-hypothalamically. Top: the projection of a representative neuron in each type; bottom: all axon projections of neurons in each type. **f**, Dot plot depicting selective projections of each type (row) in each brain area (column). The dot circle's size and color intensity indicate the percentage of neurons in each type that projected to the indicated brain area and the average projection length (in μm) in a heatmap fashion, respectively, with the scale on the right. (c) in (c)MEA and (c)CEA indicates contralateral projections. **g**, The number of *Agrp* and *Pomc* neurons in each projectome type.

https://doi.org/10.1038/s41593-025-01919-0

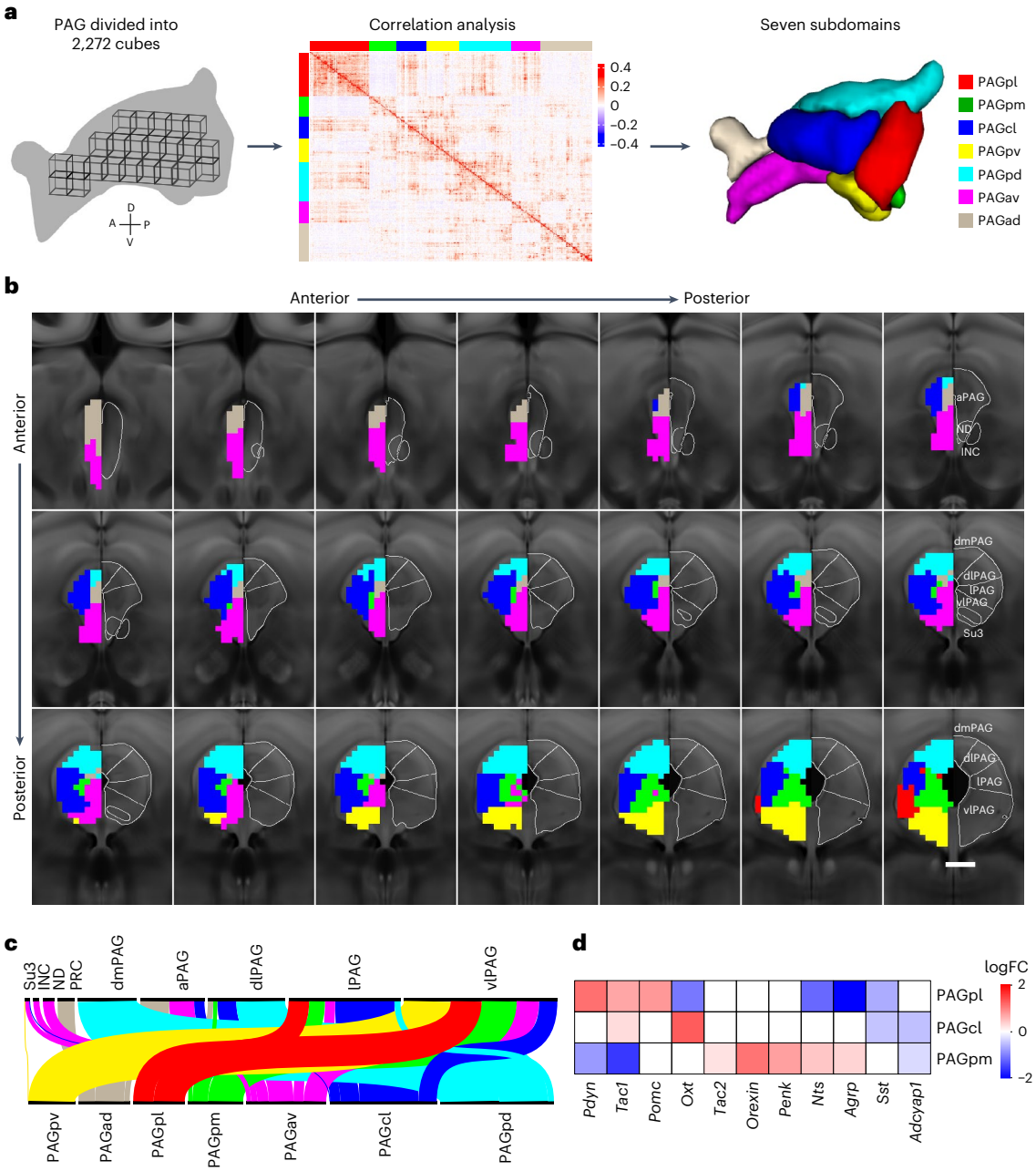

Fig. 7 | Distinct PAG subdomains defined by co-innervation patterns of hypothalamic peptidergic axons. a, We divided the PAG into 2,272 100-µm-size cubes and calculated the pairwise inter-cube correlation of hypothalamic projections. Seven modules (color-coded) showed higher intra-module than inter-module correlation of hypothalamic axon projections. These seven subdomains were plotted in a 3D view of the PAG. ad, anterior-dorsal; av, anterior-ventral; pm, posterior-medial; cl, centro-lateral; pd, posterior-dorsal; pl, posterior-lateral; pv, posterior-ventral. **b**, The seven newly defined PAG subdomains in **a** are plotted onto the 2D view of PAG for comparison with previous PAG nuclei/columns defined by the Paxinos atlas. **c**, Schematics show correspondence between the newly defined PAG subdomains with atlas-defined PAG columns/nuclei. **d**, Heatmap representation illustrating the enrichment of neuropeptide projections across the three newly defined PAG subdomains (rows). $\log_2$ fold change (logFC) values with significant changes ($P < 0.05$) are shown.

three PAG subdomains. For example, ARH *Pomc* neurons preferentially projected to the newly identified posterior-lateral PAG subdomain (PAGpl), whereas LHA *Orexin* preferred the posterior-medial PAG subdomain (PAGpm) (Fig. 7d and Extended Data Fig. 10b), suggesting a potential functional distinction between these two adjacent PAG subdomains. Taken together, this single-cell projectome analysis provides insight into the organizational principles of hypothalamic projections in the PAG and offers a distinct perspective on the structural layout and functional units within the PAG.

Structured subnetwork organization of intra-hypothalamic projections

A further outcome of our single-neuron projectome analysis was the elucidation of extensive intra-hypothalamic connectivity (Fig. 1f), which is well known but difficult to characterize by bulk tracing methods due to the small size and the densely packed organization of the hypothalamus. In our dataset, the registered intra-hypothalamic projections covered 83.6% of the ipsilateral volume and 25.7% of the contralateral volume of the hypothalamus (at the 10 µm × 10 µm × 10 µm voxel

https://doi.org/10.1038/s41593-025-01919-0

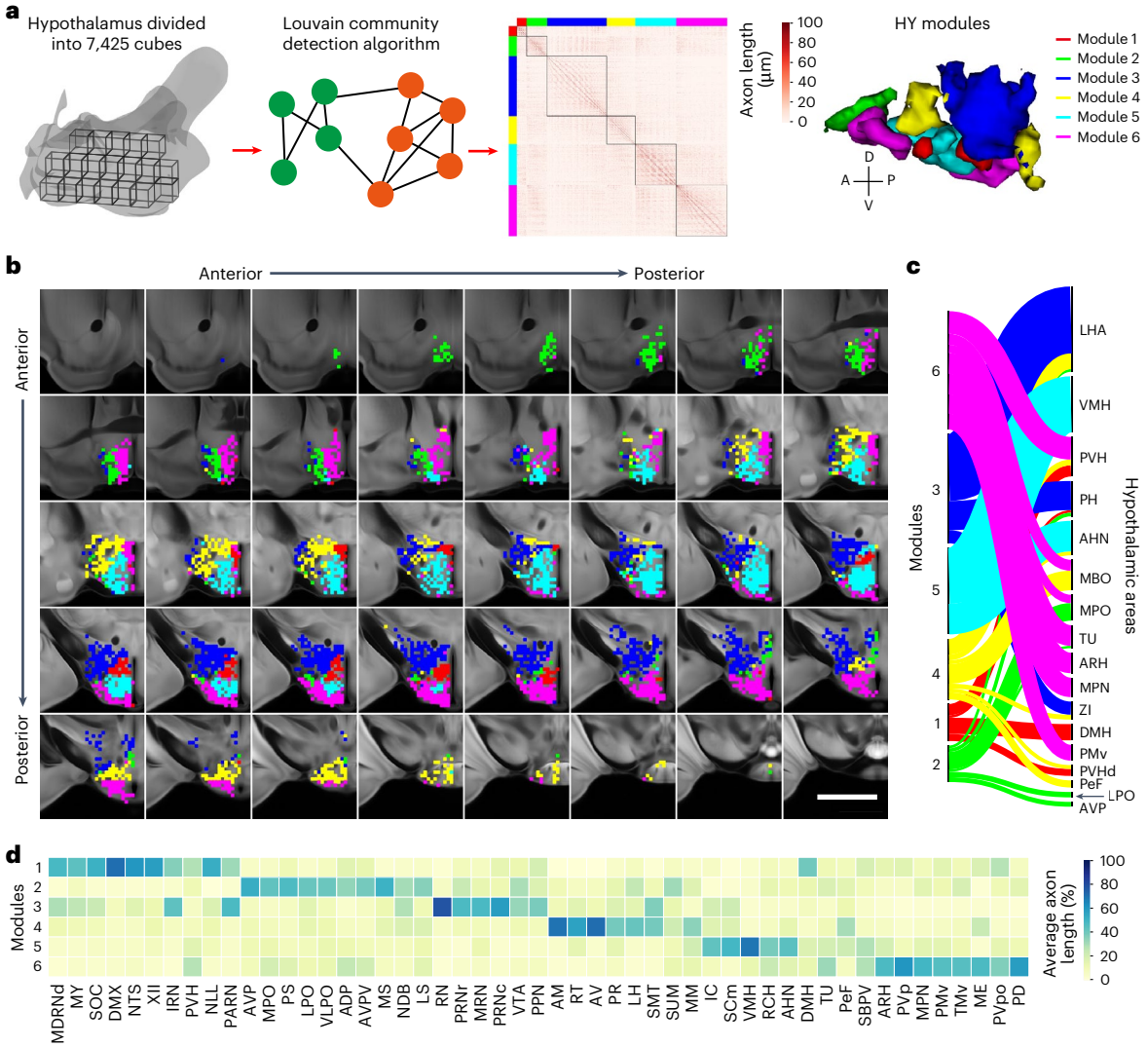

Fig. 8 | Modular subnetwork organization of intra-hypothalamic projections. **a**, Schematics illustrate the procedure for identifying hypothalamic subnetwork modules enriched for intra-modular connectivity. In brief, the brain volume of the hypothalamus was divided into 7,425 cubes, and sets of cubes enriched for intra-cube reciprocal connections were identified using the Louvain community detection algorithm. In total, six hypothalamic subnetwork modules (color-coded) were identified. **b**, The 6 hypothalamic subnetwork modules are plotted in serial coronal sections spaced 100 μm apart. Scale bar, 500 μm. **c**, Correspondence between identified subnetwork modules and anatomically defined hypothalamic nuclei. **d**, Heatmap representing the percentage of the total axon projections in a target area from each hypothalamic subnetwork module. AVP, anteroventral preoptic nucleus; MDRNd, medullary reticular nucleus, dorsal part; SOC, superior olivary complex; DMX, dorsal motor nucleus of the vagus nerve; XII, hypoglossal nucleus; NLL, nucleus of the lateral lemniscus; PS, parastrial nucleus; VLPO, ventrolateral preoptic nucleus; ADP, anterodorsal preoptic nucleus; RN, red nucleus; PRNc, pontine reticular nucleus, caudal part; RT, reticular nucleus of the thalamus; AV, anteroventral nucleus of thalamus; PR, perireunensis nucleus; SMT, submedial nucleus of the thalamus; SUM, supramammillary nucleus; RCH, retrochiasmatic area; PVpo, periventricular hypothalamic nucleus, preoptic part; PD, posterodorsal preoptic nucleus.

resolution), respectively, providing a comprehensive high-resolution view of the intra-hypothalamic connectivity and permitting us to explore the network structure of intra-hypothalamic connectivity patterns. To further analyze this, we divided the hypothalamus into 7,425 cubes of 100 μm × 100 μm × 100 μm in size, among which 3,445 contained at least one soma. Using the Louvain algorithm previously described[26], we constructed a network of intra-hypothalamic connectivity based on reciprocal projections between the cubes that contained both soma and axon (Fig. 8a).

We found that intra-hypothalamic connectivity could be characterized by six subnetworks enriched with recurrent intra-subnetwork connections (Fig. 8a). Mapping these subnetwork modules onto the brain template showed that each module corresponded to a distinct set of hypothalamic nuclei, with the prominence of a few: DMH and PVH in module 1, MPO and lateral preoptic area (LPO) in module 2, LHA and posterior hypothalamic nucleus (PH) in module 3, LHA and MBO in module 4, VMH and AHN in module 5 and medial preoptic nucleus (MPN), ARH and ventral premammillary nucleus (PMv) in module 6 (Fig. 8b,c). In support of the notion that these modular subnetworks may be functionally relevant, we found that modules 5 and 6 corresponded well to the known hypothalamic 'defensive' and 'reproductive' networks. Moreover, module 6 also placed ARH in the 'reproductive' network of the hypothalamus (Fig. 8b,c). The functional importance of these modules was further supported by the distinct preference for the downstream targets (Fig. 8d). We surmise that this modular subnetwork of intra-hypothalamic connections may organize hypothalamic outputs for regulating physiological function and innate behaviors.

Discussion

Despite the recognized importance and complexity of hypothalamic peptidergic neurons, their axonal projection patterns had not been characterized at a scale or resolution similar to single-cell transcriptome analysis. The present study addresses this gap by constructing an extensive dataset of whole-brain projectomes from over 7,000 hypothalamic neurons, each expressing one of 16 restrictedly or broadly expressed neuropeptides, with their soma spanning most hypothalamic regions. Our analysis yielded several insights into the organization of hypothalamic peptidergic axons.

We found that many hypothalamic peptidergic neurons exhibit extensive axon collateralization and arborization, enabling a single axon to simultaneously innervate multiple brain areas, corresponding regions in both hemispheres and distinct subdomains within a given area. Although previous retrograde tracing studies identified hypothalamic neurons projecting to single prominent downstream targets[50,55], our anterograde tracing method, which directly labels and detects axon arbors across the entire brain, rarely uncovered single-target axon projections. This raises concerns about potential biases in retrograde tracing methods. Notably, analysis based on total arbor length or synaptic site counts over a target yielded similar evidence of extensive collateralization. Additionally, this conclusion was supported by the analysis of hypothalamic neurons previously reported in the MouseLight project[34] (Supplementary Fig. 4). Thus, extensive axon collateralization likely represents a fundamental principle of hypothalamic projections.

Moreover, we found that there is a lack of a simple one-to-one correspondence between projectome-defined and transcriptome-defined types. Instead, some neuropeptides, which mark individual transcriptome-defined neuron types (for example, LHA *Orexin*), comprise multiple projectome-defined types. Conversely, each projectome type expressed multiple neuropeptides in distinct combinations, with preferential enrichment of a few. Similar combinatorial correspondence between projectome-defined and transcriptome-defined types was also observed for prefrontal cortex (PFC) projection neurons[26]. Thus, axon projection and gene expression patterns reflect different yet interdependent facets of neuronal features. Neurons with similar transcription profiles may serve distinct functions by projecting to different downstream targets (divergence), whereas neurons differing in transcription profiles may engage in similar biological functions by targeting the same downstream regions (convergence).

Intriguingly, we identified topographic organizations of hypothalamic axons at specific target sites for distinct peptidergic populations. For example, different MBO peptidergic populations exhibit distinct topographic axon organizations in the ATN, implying specialized roles for different neuropeptides. Furthermore, the potential implications of co-releasing classical neurotransmitters by these MBO peptidergic neurons in distinct ATN subdomains remain to be elucidated. Notably, topographic organizations of axons were also observed for other neurons, such as those *Nts*-expressing neurons in the STN/PSTN and CA1-projecting neurons expressing *Penk* or *Adcyap1*. These results suggest that topographic axon organization might be a feature in many hypothalamic peptidergic populations, indicating a vast territory for exploring and understanding hypothalamic projections and functions.

Additionally, the unprecedented resolution in our study provided important new information in characterizing the organization patterns of intra-hypothalamic connectivity, which was previously unattainable[56]. We found six modular subnetworks enriched with intra-modular reciprocal projections. Two of the six identified modules roughly matched the previously known hypothalamic 'defensive' and 'reproductive' networks[57–59], in which the synaptic connections were electrophysiologically validated[60]. Whether neurons in other newly identified modules are synaptically or functionally connected remains to be examined. Modular subnetworks generally allow localized information processing before more global integration[61]. Identifying these other modular subnetworks within the hypothalamus indicates potential functional specializations of distinct hypothalamic subdomains, which may facilitate the instantiation of internal brain states[62], such as arousal or emotion states, associated with hypothalamic activation. These hypotheses await future functional validation.

Finally, considering the hypothalamus as an example of subcortical structures, our work illustrates the complexity of both long-range projections and local connections and their potential relevance for understanding the neural circuit function of the subcortical structure. As our single-neuron tracing is restricted to axon projections, mapping the input connections to each hypothalamic neuron type is required to delineate the complete connectivity of neurons within the neural network, which is necessary to fully understand their functional roles in the future. Further integration of transcriptomic and other x-omic information into the connectivity-defined types will allow complete characterization of distinct neuronal types marked by molecular and connectivity features. To accomplish this goal, we advocate using a consensual annotation framework[27] to facilitate the integration of information generated in different laboratories. These analyses of neuronal types, coupled with immediate early gene analysis and functional manipulation, would eventually reveal how coordinated hypothalamic neuronal activities give rise to behavioral and physiological changes in the body.

Online content

Any methods, additional references, Nature Portfolio reporting summaries, source data, extended data, supplementary information, acknowledgements, peer review information; details of author contributions and competing interests; and statements of data and code availability are available at https://doi.org/10.1038/s41593-025-01919-0.

References

1. Biörklund, A., Hökfelt, T. & Swanson, L. W. *Integrated Systems of the CNS, Part I: Hypothalamus, Hippocampus, Amygdala, Retina* (Elsevier Science, 1987).
2. Saper, C. B. & Lowell, B. B. The hypothalamus. *Curr. Biol.* **24**, R1111–R1116 (2014).
3. Simerly, R. B. in *The Rat Nervous System* 4th edn (ed. Paxinos, G.) Ch. 13 (Elsevier, 2015).
4. Puelles, L., Martinez-de-la-Torre, M., Bardet, S. & Rubenstein, J. L. R. in *The Mouse Nervous System* (eds Watson, C., Paxinos, G. & Puelles, L.) Ch. 8 (Academic Press, 2012).
5. Hoyle, C. H. Neuropeptide families and their receptors: evolutionary perspectives. *Brain Res.* **848**, 1–25 (1999).
6. Van Den Pol, A. N. Neuropeptide transmission in brain circuits. *Neuron* **76**, 98–115 (2012).
7. Canteras, N. S., Simerly, R. B. & Swanson, L. W. Projections of the ventral premammillary nucleus. *J. Comp. Neurol.* **324**, 195–212 (1992).
8. Canteras, N. S., Simerly, R. B. & Swanson, L. W. Organization of projections from the ventromedial nucleus of the hypothalamus: a *Phaseolus vulgaris*-leucoagglutinin study in the rat. *J. Comp. Neurol.* **348**, 41–79 (1994).
9. Canteras, N. S. & Swanson, L. W. Projections of the ventral subiculum to the amygdala, septum, and hypothalamus: a PHAL anterograde tract-tracing study in the rat. *J. Comp. Neurol.* **324**, 180–194 (1992).
10. Goto, M., Canteras, N. S., Burns, G. & Swanson, L. W. Projections from the subfornical region of the lateral hypothalamic area. *J. Comp. Neurol.* **493**, 412–438 (2005).
11. Risold, P. Y., Canteras, N. S. & Swanson, L. W. Organization of projections from the anterior hypothalamic nucleus: a *Phaseolus vulgaris*-leucoagglutinin study in the rat. *J. Comp. Neurol.* **348**, 1–40 (1994).

12. Risold, P. Y., Thompson, R. H. & Swanson, L. W. The structural organization of connections between hypothalamus and cerebral cortex. *Brain Res. Rev.* **24**, 197–254 (1997).
13. Thompson, R. H., Canteras, N. S. & Swanson, L. W. Organization of projections from the dorsomedial nucleus of the hypothalamus: a PHA-L study in the rat. *J. Comp. Neurol.* **376**, 143–173 (1996).
14. Thompson, R. H. & Swanson, L. W. Organization of inputs to the dorsomedial nucleus of the hypothalamus: a reexamination with Fluorogold and PHAL in the rat. *Brain Res. Brain Res. Rev.* **27**, 89–118 (1998).
15. Peyron, C. et al. Neurons containing hypocretin (orexin) project to multiple neuronal systems. *J. Neurosci.* **18**, 9996–10015 (1998).
16. Wang, D. et al. Whole-brain mapping of the direct inputs and axonal projections of POMC and AgRP neurons. *Front. Neuroanat.* **9**, 40 (2015).
17. Biglari, N. et al. Functionally distinct POMC-expressing neuron subpopulations in hypothalamus revealed by intersectional targeting. *Nat. Neurosci.* **24**, 913–929 (2021).
18. Quarta, C. et al. POMC neuronal heterogeneity in energy balance and beyond: an integrated view. *Nat. Metab.* **3**, 299–308 (2021).
19. Bittencourt, J. C. Anatomical and functional heterogeneity of 'hypothalamic' peptidergic neuron populations. *Nat. Rev. Endocrinol.* **18**, 450–450 (2022).
20. Steuernagel, L. et al. HypoMap—a unified single-cell gene expression atlas of the murine hypothalamus. *Nat. Metab.* **4**, 1402–1419 (2022).
21. Yao, Z. et al. A high-resolution transcriptomic and spatial atlas of cell types in the whole mouse brain. *Nature* **624**, 317–332 (2023).
22. Langlieb, J. et al. The molecular cytoarchitecture of the adult mouse brain. *Nature* **624**, 333–342 (2023).
23. Li, H. et al. Single-neuron projectomes of mouse paraventricular hypothalamic nucleus oxytocin neurons reveal mutually exclusive projection patterns. *Neuron* **112**, 1081–1099 (2024).
24. Gong, H. et al. High-throughput dual-colour precision imaging for brain-wide connectome with cytoarchitectonic landmarks at the cellular level. *Nat. Commun.* **7**, 12142 (2016).
25. Qiu, S. et al. Whole-brain spatial organization of hippocampal single-neuron projectomes. *Science* **383**, eadj9198 (2024).
26. Gao, L. et al. Single-neuron projectome of mouse prefrontal cortex. *Nat. Neurosci.* **25**, 515–529 (2022).
27. Wang, Q. et al. The Allen Mouse Brain Common Coordinate Framework: a 3D reference atlas. *Cell* **181**, 936–953 (2020).
28. Sunkin, S. M. et al. Allen Brain Atlas: an integrated spatio-temporal portal for exploring the central nervous system. *Nucleic Acids Res.* **41**, D996–D1008 (2013).
29. Costa, M., Manton, J. D., Ostrovsky, A. D., Prohaska, S. & Jefferis, G. S. NBLAST: rapid, sensitive comparison of neuronal structure and construction of neuron family databases. *Neuron* **91**, 293–311 (2016).
30. Peng, H. et al. Morphological diversity of single neurons in molecularly defined cell types. *Nature* **598**, 174–181 (2021).
31. Mizrahi, A. et al. Comparative analysis of dendritic architecture of identified neurons using the Hausdorff distance metric. *J. Comp. Neurol.* **422**, 415–428 (2000).
32. Engelmann, M., Landgraf, R. & Wotjak, C. T. The hypothalamic–neurohypophysial system regulates the hypothalamic–pituitary–adrenal axis under stress: an old concept revisited. *Front. Neuroendocrinol.* **25**, 132–149 (2004).
33. Swaab, D. F., Pool, C. W. & Nijveldt, F. Immunofluorescence of vasopressin and oxytocin in the rat hypothalamo-neurohypophyseal system. *J. Neural Transm.* **36**, 195–215 (1975).
34. Winnubst, J. et al. Reconstruction of 1,000 projection neurons reveals new cell types and organization of long-range connectivity in the mouse brain. *Cell* **179**, 268–281 (2019).
35. Xu, S. et al. Behavioral state coding by molecularly defined paraventricular hypothalamic cell type ensembles. *Science* **370**, eabb2494 (2020).
36. Wang, Y. et al. EASI-FISH for thick tissue defines lateral hypothalamus spatio-molecular organization. *Cell* **184**, 6361–6377 (2021).
37. Lanciego, J. L., Luquin, N. & Obeso, J. A. Functional neuroanatomy of the basal ganglia. *Cold Spring Harb. Perspect. Med.* **2**, a009621 (2012).
38. Wallen-Mackenzie, A. et al. Spatio-molecular domains identified in the mouse subthalamic nucleus and neighboring glutamatergic and GABAergic brain structures. *Commun. Biol.* **3**, 338 (2020).
39. Kita, H. & Kitai, S. T. Efferent projections of the subthalamic nucleus in the rat: light and electron microscopic analysis with the PHA-L method. *J. Comp. Neurol.* **260**, 435–452 (1987).
40. Sato, F., Parent, M., Levesque, M. & Parent, A. Axonal branching pattern of neurons of the subthalamic nucleus in primates. *J. Comp. Neurol.* **424**, 142–152 (2000).
41. Fanselow, M. S. & Dong, H. W. Are the dorsal and ventral hippocampus functionally distinct structures? *Neuron* **65**, 7–19 (2010).
42. Dillingham, C. M., Frizzati, A., Nelson, A. J. & Vann, S. D. How do mammillary body inputs contribute to anterior thalamic function? *Neurosci. Biobehav. Rev.* **54**, 108–119 (2015).
43. Hou, Y. et al. Topographical organization of mammillary neurogenesis and efferent projections in the mouse brain. *Cell Rep.* **34**, 108712 (2021).
44. Jbabdi, S., Sotiropoulos, S. N. & Behrens, T. E. The topographic connectome. *Curr. Opin. Neurobiol.* **23**, 207–215 (2013).
45. Thivierge, J. P. & Marcus, G. F. The topographic brain: from neural connectivity to cognition. *Trends Neurosci.* **30**, 251–259 (2007).
46. Sakurai, T. The role of orexin in motivated behaviours. *Nat. Rev. Neurosci.* **15**, 719–731 (2014).
47. Sternson, S. M. & Eiselt, A.-K. Three pillars for the neural control of appetite. *Annu. Rev. Physiol.* **79**, 401–423 (2017).
48. Toda, C., Santoro, A., Kim, J. D. & Diano, S. POMC neurons: from birth to death. *Annu. Rev. Physiol.* **79**, 209–236 (2017).
49. Tervo, D. G. et al. A designer AAV variant permits efficient retrograde access to projection neurons. *Neuron* **92**, 372–382 (2016).
50. Betley, J. N., Cao, Z. F. H., Ritola, K. D. & Sternson, S. M. Parallel, redundant circuit organization for homeostatic control of feeding behavior. *Cell* **155**, 1337–1350 (2013).
51. Bandler, R. & Shipley, M. T. Columnar organization in the midbrain periaqueductal gray: modules for emotional expression? *Trends Neurosci.* **17**, 379–389 (1994).
52. Koutsikou, S., Apps, R. & Lumb, B. M. Top down control of spinal sensorimotor circuits essential for survival. *J. Physiol.* **595**, 4151–4158 (2017).
53. Tovote, P. et al. Midbrain circuits for defensive behaviour. *Nature* **534**, 206–212 (2016).
54. Han, W. et al. Integrated control of predatory hunting by the central nucleus of the amygdala. *Cell* **168**, 311–324 (2017).
55. Kohl, J. et al. Functional circuit architecture underlying parental behaviour. *Nature* **556**, 326–331 (2018).
56. Hahn, J. D., Sporns, O., Watts, A. G. & Swanson, L. W. Macroscale intrinsic network architecture of the hypothalamus. *Proc. Natl Acad. Sci. USA* **116**, 8018–8027 (2019).
57. Canteras, N. S. The medial hypothalamic defensive system: hodological organization and functional implications. *Pharmacol. Biochem. Behav.* **71**, 481–491 (2002).
58. Swanson, L. W. Cerebral hemisphere regulation of motivated behavior. *Brain Res.* **886**, 113–164 (2000).

59. Choi, G. B. et al. Lhx6 delineates a pathway mediating innate reproductive behaviors from the amygdala to the hypothalamus. *Neuron* **46**, 647–660 (2005).
60. Stagkourakis, S. et al. A neural network for intermale aggression to establish social hierarchy. *Nat. Neurosci.* **21**, 834–842 (2018).
61. Park, H.-J. & Friston, K. Structural and functional brain networks: from connections to cognition. *Science* **342**, 1238411 (2013).
62. Anderson, D. J. Circuit modules linking internal states and social behaviour in flies and mice. *Nat. Rev. Neurosci.* **17**, 692–704 (2016).

Zhuolei Jiao[1,16], Taosha Gao[1,16], Xiaofei Wang[1], Ao Wang[1,2], Yawen Ma[1], Li Feng[1], Le Gao[1], Lingfeng Gou[1], Wen Zhang[1], Nasim Biglari[3,4,5], Emma E. Boxer[6,7], Lukas Steuernagel[3,4,5], Xiaojing Ding[1], Zixian Yu[1,2], Mingjuan Li[1,2], Mengtong Gao[1], Mingkun Hao[1], Hua Zhou[1], Xuanzi Cao[1], Shuaishuai Li[1,2], Tao Jiang[8], Jiamei Qi[8], Xueyan Jia[8], Zhao Feng[8], Biyu Ren[1], Yu Chen[1], Xiaoxue Shi[1], Dan Wang[1], Xinran Wang[1], Luyao Han[1], Yikai Liang[1], Liuqin Qian[1], Chenxi Jin[1], Jiawen Huang[1], Wei Deng[1], Congcong Wang[1], E Li[1], Yue Hu[1], Zi Tao[1], Humingzhu Li[1,9], Xiang Yu[1,10], Min Xu[1], Hung-Chun Chang[1], Yifeng Zhang[1], Huatai Xu[1], Jun Yan[1], Anan Li[8], Qingming Luo[8,11], Ron Stoop[12], Scott M. Sternson[13], Jens C. Brüning[3,4,5], David J. Anderson[6,7], Mu-ming Poo[1], Yidi Sun[1] ✉, Shengjing Xu[1] ✉, Hui Gong[8] ✉, Yan-Gang Sun[1,14] ✉ & Xiaohong Xu[1,15] ✉

[1]Institute of Neuroscience, CAS Center for Excellence in Brain Science and Intelligence Technology, Chinese Academy of Sciences, Shanghai, China. [2]University of Chinese Academy of Sciences, Beijing, China. [3]Max Planck Institute for Metabolism Research, Cologne, Germany. [4]Policlinic for Endocrinology, Diabetology and Preventive Medicine, University of Cologne, Faculty of Medicine and University Hospital Cologne, Cologne, Germany. [5]Cluster of Excellence in Cellular Stress Responses in Aging-associated Diseases (CECAD), Cologne, Germany. [6]Division of Biology and Biological Engineering, California Institute of Technology, Pasadena, CA, USA. [7]Howard Hughes Medical Institute; Tianqiao and Chrissy Chen Institute for Neuroscience, California Institute of Technology, Pasadena, CA, USA. [8]HUST-Suzhou Institute for Brainsmatics, JITRI, Suzhou, China. [9]School of Life Science and Technology, ShanghaiTech University, Shanghai, China. [10]School of Life Sciences, Peking-Tsinghua Center for Life Sciences and Peking University McGovern Institute, Peking University, Beijing, China. [11]Key Laboratory of Biomedical Engineering of Hainan Province, School of Biomedical Engineering, Hainan University, Haikou, China. [12]Department of Psychiatry, Center for Psychiatric Neuroscience, Lausanne University Hospital Center (CHUV) and University of Lausanne (UNIL), Lausanne, Switzerland. [13]Department of Neurosciences, Howard Hughes Medical Institute, University of California, San Diego, La Jolla, CA, USA. [14]Key Laboratory of Brain Cognition and Brain-inspired Intelligence Technology, Chinese Academy of Sciences, Shanghai, China. [15]State Key Laboratory of Medical Neurobiology and MOE Frontiers Center for Brain Science, Institutes of Brain Science, Fudan University, Shanghai, China. [16]These authors contributed equally: Zhuolei Jiao, Taosha Gao. ✉e-mail: ydsun@ion.ac.cn; sxu@ion.ac.cn; huigong@brainsmatics.org; yangang.sun@ion.ac.cn; xiaohongxu46@gmail.com

Methods

Animals

Genetically modified mouse lines, including *Adcyap1-2A-Cre* (B6.Cg-Adcyap1$^{tm1.1(cre)Hze}$/ZakJ, catalog number 030155), *Agrp-IRES-Cre* (STOCK Agrp$^{tm1(cre)Lowl}$/J, catalog number 012899), *Avp-IRES-Cre* (B6.Cg-Avp$^{tm1.1(cre)Hze}$/J, catalog number 023530), *Crh-IRES-Cre* (B6(Cg)-Crh$^{tm1(cre)Zjh}$/J, catalog number 012704), *Nts-IRES-Cre* (B6;129-Nts$^{tm1(cre)Mgmj}$/J, catalog number 017525), *Oxytocin-IRES-Cre* (B6;129S-Oxt$^{tm1.1(cre)Dolsn}$/J, catalog number 024234), *Pdyn-IRES-Cre* (B6;129S-Pdyn$^{tm1.1(cre)Mjkr}$/LowlJ, catalog number 027958), *Penk-IRES-Cre* (B6;129S-Penk$^{tm2(cre)Hze}$/J, catalog number 025112), *Pmch-Cre* (STOCK Tg(Pmch-cre)1Lowl/J, catalog number 014099), *Pomc-Cre* (STOCK Tg(Pomc1-cre)16Lowl/J, catalog number 005965), *Sst-IRES-Cre* (STOCK Sst$^{tm2.1(cre)Zjh}$/J, catalog number 018973), *Tac1-IRES-Cre* (B6;129S-Tac1$^{tm1.1(cre)Hze}$/J, catalog number 021877), *Tac2-Cre* (B6.129-Tac2$^{tm1.1(cre)Qima}$/J, catalog number 018938), *Trh-IRES-Cre* (B6;129S-Trh$^{tm1.1(cre)Mjkr}$/LowlJ, catalog number 032468), *Vip-IRES-Cre* (STOCK Vip$^{tm1(cre)Zjh}$/J, catalog number 010908) and *LSL-h2b-GFP* (STOCK Gt(ROSA)26Sort$^{m8(CAG-HIST1H2BB/EGFP)Zjh/J}$, catalog number 036761), were purchased from The Jackson Laboratory and bred in-house. Wild-type mice of the C57BL/6J background were purchased from the SLAC Laboratory. All mice were housed on a 12-h light/dark cycle with water and food ad libitum in the institute's animal facility. Only adult males older than 8 weeks of age were used in the study. All experimental protocols were approved by the Institutional Animal Care and Use Committee (IACUC) of the Center for Excellence in Brain Science and Intelligence Technology, Chinese Academy of Sciences, in Shanghai, China (IACUC number NA-016-2016).

Virus

We used various methods to achieve sparse labeling of neurons with cell type specificity. For virus injected into *Cre* animals, these methods included diluting AAVs expressing *Cre*-dependent GFPs of different versions or mixing AAVs expressing *Cre*-dependent *FlpO* and AAVs expressing *FlpO*-dependent fluorescent protein at a ratio. Viral mixing was achieved by either combining two AAVs produced separately or by co-transfection of mixed plasmid backbones for both AAVs to cells during the viral production step as described[63]. In addition, to label *Orexin* neurons, we injected AAVs encoding mNeoGreen under the control of the *Orexin* promoter (PPORX) into wild-type males.

Several viruses were used in this study. AAV–CAG–DIO–FlpO (titer, 5.0×10^9 genomic copies per milliliter (gc ml^{-1})) was purchased from Shanghai Taitool Bioscience Co., Ltd. The JS series of virus was a mixture of AAV–hSyn Con/Fon EYFP and AAV–EF1a–FlpO generated at a different ratio during the virus-packaging step (1:4,000, titer, 5.2×10^{12} gc ml^{-1}; 1:8,000, titer, 1.41×10^{13} gc ml^{-1}; 1:40,000, titer, 5.1×10^{12} gc ml^{-1}) which were purchased from Brain Case (Shenzhen) Biotechnology Co., Ltd. AAV–EF1a–fDIO–EYFP (titer, 1.31×10^{13} gc ml^{-1}); AAV–EF1a–DIO–Ypet–2A–mGFP (titer, 2.82×10^{12} gc ml^{-1}); AAV–EF1a–DIO–FlpO (titer, 3.2×10^9 gc ml^{-1} or 4.1×10^9 gc ml^{-1} or 1×10^9 gc ml^{-1} or 4.0×10^{10} gc ml^{-1} or 1.25×10^9 gc ml^{-1}); and AAV–EF1a–fDIO–Ypet–P2A–mGFP (titer, 7.4×10^{12} gc ml^{-1} or 6.3×10^{12} gc ml^{-1} or 9.8×10^{12} gc ml^{-1} or 2.31×10^{12} gc ml^{-1} or 1.05×10^{12} gc ml^{-1} or 5.5×10^{12} gc ml^{-1}). AAV–PPORX–mNeoGreen (titer, 1.0×10^{13} gc ml^{-1}); AAV–EF1a–DIO–EYFP (titer, 1.0×10^{12} gc ml^{-1}); retroAAV–EF1α–nls–mNeoGreen viral vector (titer, 5×10^{13} gc ml^{-1}); and retroAAV–hsyn–cre–GFP (titer, 6.3×10^{12} gc ml^{-1}) were produced by the Gene Editing Core Facility at the institute.

Surgery

Stereotaxic surgeries for preparing samples for fMOST imaging were conducted by injecting AAVs into different hypothalamic nuclei according to the Paxinos and Franklin Mouse Brain Atlas (2nd edition) as previously described[23,64]. Detailed information about the AAVs injected, the injection coordinates and the injection volumes for each brain sample is provided in Supplementary Table 1. Additionally, stereotaxic surgeries for retrogradely labeling midbrain-projecting neurons, as shown in Fig. 2 and Extended Data Fig. 9, were performed by injecting AAVs into the PAG of the midbrain using the following coordinates relative to bregma: AP: −4.6 mm; ML: ±0.65 mm; DV: −2.6 mm, according to the Paxinos and Franklin Mouse Brain Atlas (2nd edition).

Histology

Animals were anesthetized with 1% pentobarbital sodium (50 mg kg^{-1}, intraperitoneally; Merck) and transcardially perfused with DEPC-treated PBS, followed by ice-cold 4% paraformaldehyde (PFA) in PBS. Brains were dissected and post-fixed in PFA overnight at 4 °C and dehydrated with 30% sucrose in DEPC-PBS. Afterwards, brains were sectioned at 20-μm thickness and mounted onto Superfrost Plus slides (Thermo Fisher Scientific, 12-550-15). After drying in the air, slides were stored at −80 °C before being processed according to the RNAscope Multiplex Fluorescent Reagent Kit v2 User Manual (ACDBio). Probes against specific peptide mRNA were ordered from ACDBio and used in the experiment. Images were captured under a ×40 objective using a confocal microscope (Nikon, C2).

fMOST imaging, tracing and registration

Imaging. The fMOST imaging was acquired as previously described[26]. In brief, the dissected brains were post-fixed in 4% PFA and then embedded in Lowicryl HM20 resin (Electron Microscopy Sciences, 14340). The resin-embedded brains were imaged in a water bath containing propidium iodide (PI) under an fMOST microscope at a voxel resolution of 0.32 μm × 0.32 μm × 1 μm. In brief, the sample surface in a coronal plane was imaged for GFP (for neuron tracing) and PI channels (for brain registration) and then removed at 1-μm step by a fixed diamond knife. The imaging–sectioning cycle was continued until the entire brain sample was fully imaged.

Tracing. A new software tool, Fast Neurite Tracer (FNT), was developed in-house to trace long-range axon projection in terabyte datasets generated by light microscopy[26]. In brief, the original image data are split into smaller three-dimensional (3D) data cubes by a program called 'slice2cube' in FNT. At any time, approximately eight neighboring cubes around a position are loaded into computer memory automatically and visualized in 3D for tracing. The tracing process involves finding a putative path, examining the path and extending the current neurite tree. At each step, confirmation from a user is required to proceed, thereby ensuring the correctness of tracing. An axon projection can be traversed in this way until completion. Different neurons in the same sample were traced by different personnel in parallel and cross-validated after completion. In addition, each traced neuron was independently checked by another person to ensure accuracy, and each brain sample was subjected to random post-tracing quality checks.

Registration. The whole brain with information from all reconstructed neurons was registered into the standard Allen CCFv3 (ref. 27) using a previously described method[26]. In brief, we segmented several brain regions as landmarks through cytoarchitecture references. We performed diffeomorphic transformation and symmetric image normalization in Advanced Normalization Tools (ANTs) to acquire transformation parameters based on these landmarks. These transformation parameters were applied to all the traced neurons within the brain sample to remap the reconstructed neuron onto the Allen brain template.

Data analysis

Neuron exclusion. All neurons were manually checked to ensure that they were correctly traced. Neurons found to have erroneous tracing data were excluded from further analysis. Additionally, neurons whose soma location was outside the hypothalamus were also excluded for clustering analysis. In total, we included 7,180 neurons in our analysis with neuronal cell body located in the Allen CCFv3-defined

hypothalamus. We mirrored all neurons to the same hemisphere before the analysis procedures.

Parameter calculation. Based on the standard Allen CCFv3 annotation file (http://download.alleninstitute.org/informatics-archive/current-release/mouse_ccf/annotation/ccf_2017/), we calculated the soma location, axon length and terminal number for each neuron in each brain region using a self-developed Python library (https://pypi.org/project/pyswcloader/). To analyze and show the data in a more reader-friendly way, we manually combined some brain areas into larger ones.

Calculating the total brain volume occupation. We divided the standard mouse brain (CCFv3) into small cubes of 25 μm × 25 μm × 25 μm. Subsequently, we determined whether each cube has an axon projection signal from the 7,180 reconstructed neurons. We found that the total axon arbors of these peptidergic neurons extended to occupy approximately 21.8% and 10.2% of the voxels on the ipsilateral and contralateral sides of the brain, respectively.

Neuron visualization. All 3D neuron showcases were plotted using a self-developed Python package, 'neuron-vis' (https://gitee.com/bigduduwxf/neuron-vis). Colors were randomly assigned to individual neurons plotted at a population level. For zoom-in views of the axon projections in particular areas in a two-dimensional (2D) view, we picked three neurons in each type that had the highest axon length in the chosen brain region and plotted their axons on the center coronal section of the brain region in the Allen template brain.

Projectome-based neuron classification. We calculated a modified Hausdorff match distance[31] as the similarity index of neuron pairs in our dataset. In brief, we broke each neuron trace into sets of evenly spaced points in the 3D Allen template brain space to generate two sets of points for a neuron pair, A and B. For a given point '*i*' in the set A, we then calculated all the distances to every single point in the set B and picked out the smallest value—that is, the closest distance to neuron B. This value is defined as $d(A_i, B)$. We re-iterated this process for all points on neuron A, generating a collection of $d(A_{i1\to j}, B)$, defined as $D(A, B)$, from which we calculated the mean and the maximum value of the collection. We then calculated a weighted average by taking into the consideration of the ratio, α, of points in the set A that had $d(A_i, B)$ smaller than the mean value. Thus, $d(A \to B)$ was the directional A → B distance and was calculated as $\alpha \times \text{Mean}(D(A, B)) + (1 - \alpha)) \times \text{Max}(D(A, B))$. The directional distance B → A was calculated in the same manner. The similarity index between neuron pair A and B is the mean of $d(A \to B)$ and $d(B \to A)$. The formulas are as follows:

$$d(A_i, B) = \text{Min}\|i, j\|, j \in B$$

$$D(A, B) = \bigcup_{i \in A} d(A_i, B)$$

$$d(A \to B) = \alpha \times \text{Mean}(D(A, B)) + (1 - \alpha) \times \text{Max}(D(A, B))$$

$$d(A, B) = d(B, A) = \text{Mean}(d(A \to B), d(B \to A))$$

After generating the similarity index of all neuron pairs, we performed hierarchical clustering of the matrix using Ward's linkage to identify projectome-defined neuron types. The clustering threshold was at a distance equal to or smaller than 8,000. This yielded 31 projectome-defined types.

Validation of image registration. To calculate the registration accuracy, we randomly picked four brain samples and manually labeled three brain areas in the 3D space—fimbria (fi), ME and interpeduncular nucleus (IPN)—before the registration. We then got the coordinates of these brain areas after registration, calculated the mass center and measured their Euclidean distance to the mass center of fi, ME and IPN as defined by the standard Allen brain template, to illustrate the registration accuracy.

Selection of preferentially targeted areas for each type. To select the brain areas that were preferentially targeted by a given projectome-defined type in dot plots, we compared the percentage of neurons in each type and the number of neurons in the remaining types that project to a given brain area by Fisher's exact test. We chose the target brain areas that showed the most significant differences for each type to plot.

PAG column/nucleus preference. Only axon projections in the ipsilateral PAG were considered. We first calculated axon projection density in each PAG column/nucleus and in the whole PAG by dividing the total axon projection lengths in each region by the corresponding volume. We then divided the axon projection density for each column/nucleus by that for the whole PAG to get the preference score for each domain.

Enrichment analysis. To assess the enrichment of soma location and neuropeptides within each distinct projection type, we conducted $\log_2$ fold change analysis, a method previously described[65]. In brief, the enrichment of cells with feature A within the test group is calculated as:

$$\text{log fold change} = \log_2\left(\frac{\text{Percentage of A cells in the test group} + \text{pseudocount}}{\text{Percentage of A cells in all other groups} + \text{pseudocount}}\right),$$

where we set pseudocount = 1 to avoid null value.

To minimize the risk of false-positive results, we used the Wilcoxon rank-sum test with Bonferroni correction and only presented the results with significant differences ($P < 0.05$ after correction).

Topographic analysis. To explore the topographic projection patterns of type 2, type 4 and type 22, we analyzed the correlation between the location of neuronal cell bodies and the centroids of neuron fiber terminals along the three axes (A-P, D-V and M-L) in the 3D space. Then, we employed linear regression analysis to fit these data points.

PAG subdomains defined by hypothalamic co-innervation. In the standard Allen brain template, the PAG was not subdivided to columns as in the Paxinos and Franklin Mouse Brain Atlas. We, therefore, manually annotated the PAG into four columns—dmPAG, dlPAG, vlPAG and lPAG—in the standard Allen brain template using the Paxinos and Franklin Mouse Brain Atlas as the reference. We labeled the anterior section of the PAG that was not included in the four columns as the aPAG. To analyze co-innervation patterns of individual hypothalamic neurons, we first divided the ipsilateral PAG into 2,272 cubes of 100 μm × 100 μm × 100 μm size. For each PAG-projecting neuron, we calculated its axonal project length in all 2,272 of these cubes. After obtaining the projection strength matrix, we conducted hierarchical clustering using Spearman's rank correlation coefficient as the distance measure and Ward's linkage to obtain clustered cubes receiving highly correlated hypothalamus inputs. This method identified seven PAG subdomains.

Modular subnetwork organization of intra-hypothalamic projections. To analyze the intra-hypothalamic projection patterns, we divided the hypothalamus volume into 7,425 cubes of 100 μm × 100 μm × 100 μm size, considering only the hemisphere where the soma of all neurons was located. Of these 7,425 cubes, 3,445 had both neuron and axon projections in them. We calculated the

axonal length of each neuron in these 3,445 cubes. To investigate the modular structure of connectivity, we used the Louvain community detection algorithm from the Brain Connectivity Toolbox[66] (https://sites.google.com/site/bctnet/) to find consistent modular structures within these cubes. The final modular structure was obtained at $\gamma = 1$, with six intra-hypothalamus modules identified.

scRNA-seq and MERFISH dataset of the mouse hypothalamus

scRNA-seq data were retrieved from the Neuroscience Multi-omics Archive under the following identifier: https://allen-brain-cell-atlas.s3-us-west-2.amazonaws.com/expression_matrices/WMB-10Xv3/20230630/WMB-10Xv3-HY-raw.h5ad. MERFISH data were retrieved from the available dataset[21] through the following link: https://datasets.cellxgene.cziscience.com/cf2d2ef7-558c-4d50-9c669bc-fee00d89e.h5ad. We preprocessed the dataset using Scanpy (version 1.9.6), first normalizing the total counts of each cell by 1,000 and then log normalizing the counts. The normalized counts were scaled within each gene by z-score transformation. The processed gene expression counts matrix was then subjected to dimensional reduction and clustering analyses. We reduced the dimensionality to 50 principal component analysis (PCA) dimensions and calculated the 15 nearest neighbors of each cell in the PCA space. Finally, we employed the uniform manifold approximation and projection (UMAP) algorithm to reduce the data to 2D space for visualization and further analysis.

For analysis of neuropeptide expression, gene expression matrices for the 16 neuropeptides were extracted from the normalized scRNA-seq dataset, and their average expression levels across the 1,451 neuron types in the dataset were computed. Subsequently, the mean and s.d. of gene expression count values corresponding to the 16 neuropeptides were calculated separately, and, when the expression count level of a cell is 1 s.d. above the mean value, then the cell is considered to express the neuropeptide. If 25% of cells in a given neuron type express a neuropeptide above the threshold, this neuropeptide is considered to be enriched in this cluster.

EASI-FISH sample preparation, imaging and data processing

Sample preparation. For the EASI-FISH experiments, two male C57BL/6J mice, approximately 8 weeks of age, were used. The AAVretro–EF1α–nls–mNeoGreen viral vector was diluted to a final titer of 5×10^{12} genomic copies per milliliter. A volume of 400 nl of the diluted virus was injected into the PAG using the following coordinates relative to bregma: AP: −4.6 mm; ML: ±0.65 mm; DV: −2.6 mm. Four weeks after injection, the mice were anesthetized with isoflurane and perfused sequentially with 20 ml of RNase-free PBS followed by 20 ml of ice-cold 4% PFA. The brains were then dissected, fixed in 4% PFA overnight and sectioned into 300-µm coronal slices, which were stored in 70% ethanol at 4 °C. Specific regions (0.8 mm × 0.8 mm) of the coronal slices containing the VMH were identified by visualizing mNeoGreen signals and anatomical landmarks under a fluorescence dissecting microscope. These regions were then excised for further EASI-FISH processing.

EASI-FISH was performed as previously described with minor modifications[36]. In brief, the brain slices were rehydrated in PBS and underwent RNA anchoring, gelation, proteinase K digestion and DNase I digestion. To identify midbrain-projecting neurons, mNeoGreen and cytosolic DAPI signals were acquired before in situ hybridization of the target neuropeptide genes. mNeoGreen was then bleached using a white LED in a 4 °C cold room. Two rounds of hybridization chain reaction RNA fluorescence in situ hybridization (HCR RNA-FISH) were performed to detect the expressions of four neuropeptides (round 1: *Adcyap1*-488, *Sst*-546, *Pdyn*-669; round 2: *Tac2*-669), following a previous EASI-FISH protocol.

Imaging. FISH images were acquired using a Zeiss Lightsheet 7 microscope. A ×20 water immersion objective (×20/1.0 W Plan-Apochromat Corr DIC M27 75 mm, RI = 1.33) was used for imaging with ×0.5 zoom. Images were collected at 0.468 × 0.468-µm pixel resolution (post-expansion) and 0.686-µm z-step size with single camera detection of four tracks: 405-nm, 488-nm, 560-nm and 660-nm channels. Each image tile was 898.56 µm × 898.56 µm (post-expansion) with 10% overlap between tiles.

Data processing. Three-dimensional image tiles were stitched using the ImageJ Stitching plugin[67]. Stitched 3D image volumes from each round of HCR RNA-FISH as well as from the mNeoGreen round were registered based on the DAPI signals using a customized MATLAB (MathWorks) script. To generate 3D cell boundaries, 3D cell segmentation was performed with Cellpose 2.0 based on the DAPI signal. The 3D segmentation results were further manually inspected and corrected. mRNA transcript signals were identified using a clamped Otsu's threshold (maximum (400, Otsu's)). Non-specific lipofuscin signals, detected by co-localization of signals across all FISH channels, were removed from the FISH image volumes. Three features (voxels, mean intensity and sum intensity, where sum intensity = voxels × mean intensity) of each mRNA signal were extracted from individual cells in the subtracted FISH image volumes. In Fig. 2f, to reduce batch effect, these total intensities were normalized to [0 1] by $(val\_i - val\_n\_min) / (val\_n\_max - val\_n\_min)$, where val_i is the total intensity from Neuron i, and val_n_min and val_n_max are the minimum and maximum total intensities among neurons from the same Animal n as Neuron i. In Fig. 2g, a cell was considered to express a neuropeptide if the signals met the following criteria: (1) voxels > 300 and (2) total intensity > 10th percentile of total intensities of neurons meeting criterion 1.

Statistics and reproducibility

No statistical method was used to predetermine sample size, and the experiments were not randomized. For single-neuron projectome data, Supplementary Fig. 1a shows the procedure for sample exclusion. In brief, investigators were blinded to the identity of the brain samples being processed. Brain samples with excessively dense labeling, which precludes single-axon tracing, were excluded from subsequent neuronal tracing procedures. All traced neurons underwent multiple rounds of manual verification to ensure accuracy. Neurons with erroneous tracing data were excluded from further analysis. Additionally, neurons with soma locations outside the hypothalamus were excluded unless otherwise stated. All other neurons included for analysis in the present study had explicitly stated identifiers (for example, soma location, neuropeptide population or target regions). For EASI-FISH experiments, brain slices from two independently injected male mice (biological replicates) were processed for imaging and grouped for analysis, following the standard protocol for single-neuron analysis. For all other histological studies, at least three biological replicates were obtained for each experiment. For a detailed summary of the statistical analysis, see Supplementary Table 6.

Materials availability

All unique/stable reagents generated in this study are available upon reasonable request.

Reporting summary

Further information on research design is available in the Nature Portfolio Reporting Summary linked to this article.

Data availability

The reconstructed projectome data for the 7,180 neurons are publicly accessible on our websites: https://mouse.digital-brain.cn/projectome/hy and https://www.braindatacenter.cn/datacenter/web/#/dataSet/details?id=1800731789745954817. Source data are provided with this paper.

Code availability

A Python library containing computer code used for feature calculations is available at https://pypi.org/project/pyswcloader/. Additionally, all source code for analyzing these features and for generating each figure can be found at https://zenodo.org/records/14588094 (ref. 68), which is organized according to the panels in each figure. All other data and codes are available from the corresponding authors upon reasonable request.

References

63. Sun, P. et al. Highly efficient and super-bright neurocircuit tracing using vector mixing-based virus cocktail. Preprint at *bioRxiv* https://doi.org/10.1101/705772 (2020).
64. Li, X.-Y. et al. AGRP neurons project to the medial preoptic area and modulate maternal nest-building. *J. Neurosci.* **39**, 456–471 (2019).
65. Hao, Y. et al. Dictionary learning for integrative, multimodal and scalable single-cell analysis. *Nat. Biotechnol.* **42**, 293–304 (2023).
66. Rubinov, M. & Sporns, O. Complex network measures of brain connectivity: uses and interpretations. *NeuroImage* **52**, 1059–1069 (2010).
67. Preibisch, S., Saalfeld, S. & Tomancak, P. Globally optimal stitching of tiled 3D microscopic image acquisitions. *Bioinformatics* **25**, 1463–1465 (2009).
68. Jiao, Z., Gao, T. & Xu, X. Projectome-based characterization of hypothalamic peptidergic neurons in male mice. *Zenodo* https://doi.org/10.5281/zenodo.14588094 (2025).

Acknowledgements

We thank Z. Liang for valuable discussions during paper preparation. This work was supported by the National Science and Technology Innovation 2030 Major Program (2021ZD0204400 to Y.-G.S., 2021ZD0203200-03 to X.X., 2021ZD0201000 to H.G., 2021ZD0200100 to Y.S. and 2021ZD0204401 to S.X.); the National Science Foundation of China (32321003 and 32371072 to S.X.); the Shanghai Municipal Science and Technology Major Project (2018SHZDZX05 to X.X.); and the Lingang Laboratory (LG202104-01-01 to Y.-G.S. and LG202104-01-04 to X.X.). The funders had no role in study design, data collection and analysis, preparation of the manuscript or decision to publish.

Author contributions

Conceptualization: M.-m.P., Y.-G.S. and X.X. Experiments: virus injections, X.D., Z.Y., M.L., M.H., H.Z., X.C., S.L., C.W., E.L. Y.H., Z.T. and H.L.; fMOST imaging, T.J., J.Q., X.J., Z.F., A.L., Q.L. and H.G.; EASI-FISH, A.W. and S.X.; RNAscope, X.D., M.L., M.H., H.Z., X.C., S.L., C.W., E.L., Y.H., Z.T., H.L. and M.G.; and fMOST data curation, Xinran Wang and Y.C. Data analysis: fMOST neurite tracing, L. Gou, B.R., X.S., D.W., L.H., Y.L. and Xiaofei Wang; fMOST data visualization and comparative analysis, Z.J., T.G., L. Gao, N.B., E.E.B., L.S., S.M.S., J.C.B., M.-m.P., D.J.A., J.Y. and X.X.; single-cell transcriptome analysis, Y.M., L.F. and Y.S.; and EASI-FISH data analysis, A.W., Z.J., T.G. and S.X. Website construction: L.Q., C.J., J.H. and W.D. Figure plotting: Z.J., T.G., W.Z., Z.Y. and M.L. Supervision: X.Y., M.X., H.-C.C., Y.Z., H.X., S.X., Y.S., Y.-G.S., X.X., Q.L. and H.G. Paper writing: R.S., M.-m.P. and X.X.

Competing interests

The authors declare no competing interests.

Additional information

Extended data is available for this paper at https://doi.org/10.1038/s41593-025-01919-0.

Supplementary information The online version contains supplementary material available at https://doi.org/10.1038/s41593-025-01919-0.

Correspondence and requests for materials should be addressed to Yidi Sun, Shengjing Xu, Hui Gong, Yan-Gang Sun or Xiaohong Xu.

Peer review information *Nature Neuroscience* thanks Dayu Lin and the other, anonymous, reviewer(s) for their contribution to the peer review of this work.

https://doi.org/10.1038/s41593-025-01919-0

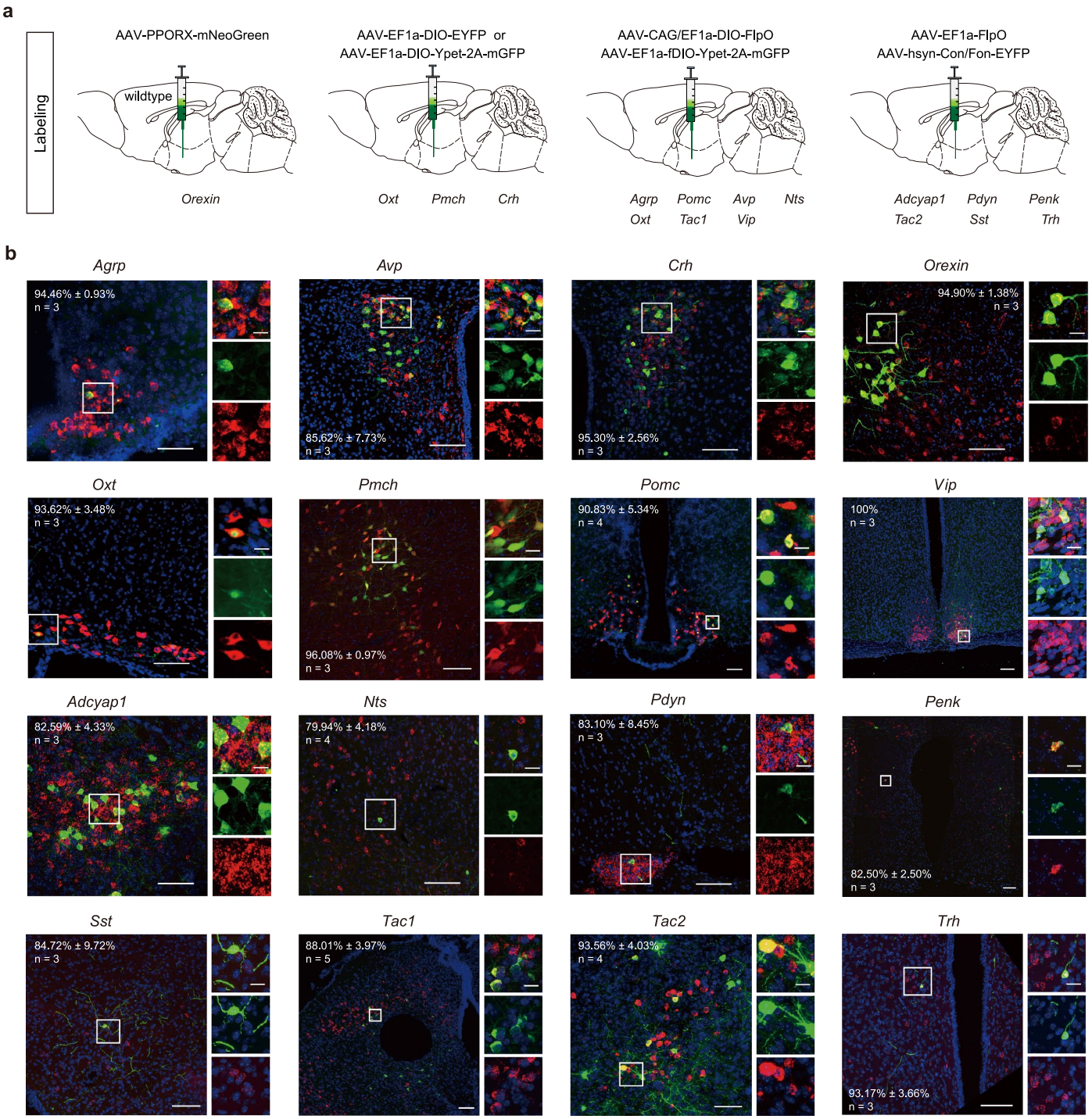

Extended Data Fig. 1 | Viral strategies for sparsely labeling hypothalamic peptidergic neurons. a. To sparsely label neuropeptide-expressing populations listed at the bottom, the indicated virus or virus mixture was injected into wild-type mice to label *Orexin*-expressing neurons or into *Cre*-expressing mice to label all other peptidergic populations. **b**. Representative images showing co-localization of EYFP or GFP signal with in situ or immunohistochemistry signals of the indicated neuropeptide (red). The quantification shows the percentage (%) of EYFP or GFP-labeled cells that co-expressed the neuropeptide. Data are presented as mean ± S.E.M. N indicates the number of biological replicates. The images on the right show magnified regions within the white box on the left. Scale bar, left, 100 µm; right, 20 µm.

https://doi.org/10.1038/s41593-025-01919-0

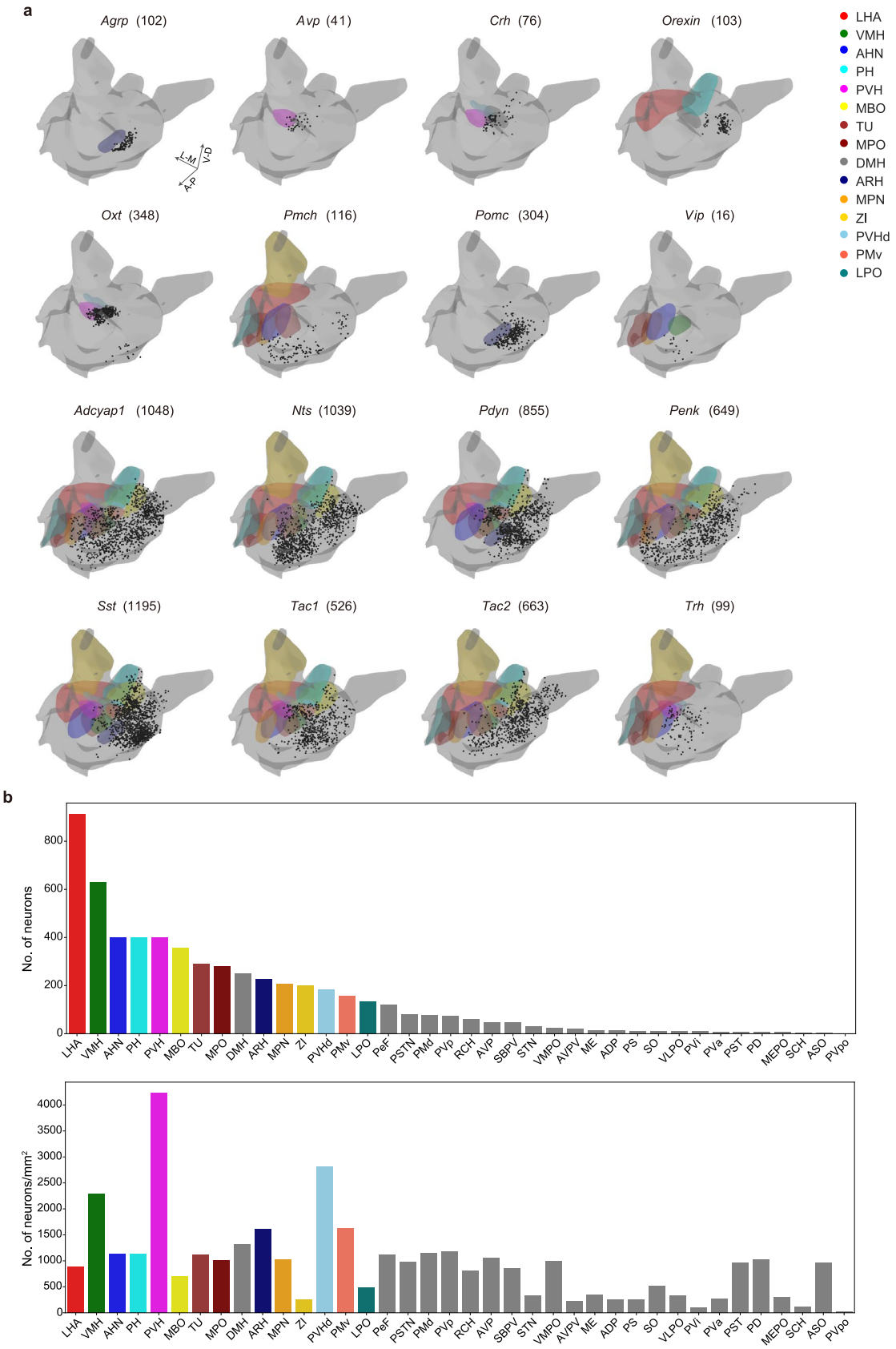

Extended Data Fig. 2 | Soma distribution of each peptidergic population. a. 3D view of the soma distribution of neurons across the 16 peptidergic populations within various hypothalamic nuclei (outlined on the contralateral side and color-coded). The number of reconstructed neurons for each peptidergic population is indicated in the parenthesis. **b**. Bar graphs showing the number (top) and the density (bottom) of reconstructed neurons with somas located in the indicated hypothalamic nuclei.

https://doi.org/10.1038/s41593-025-01919-0

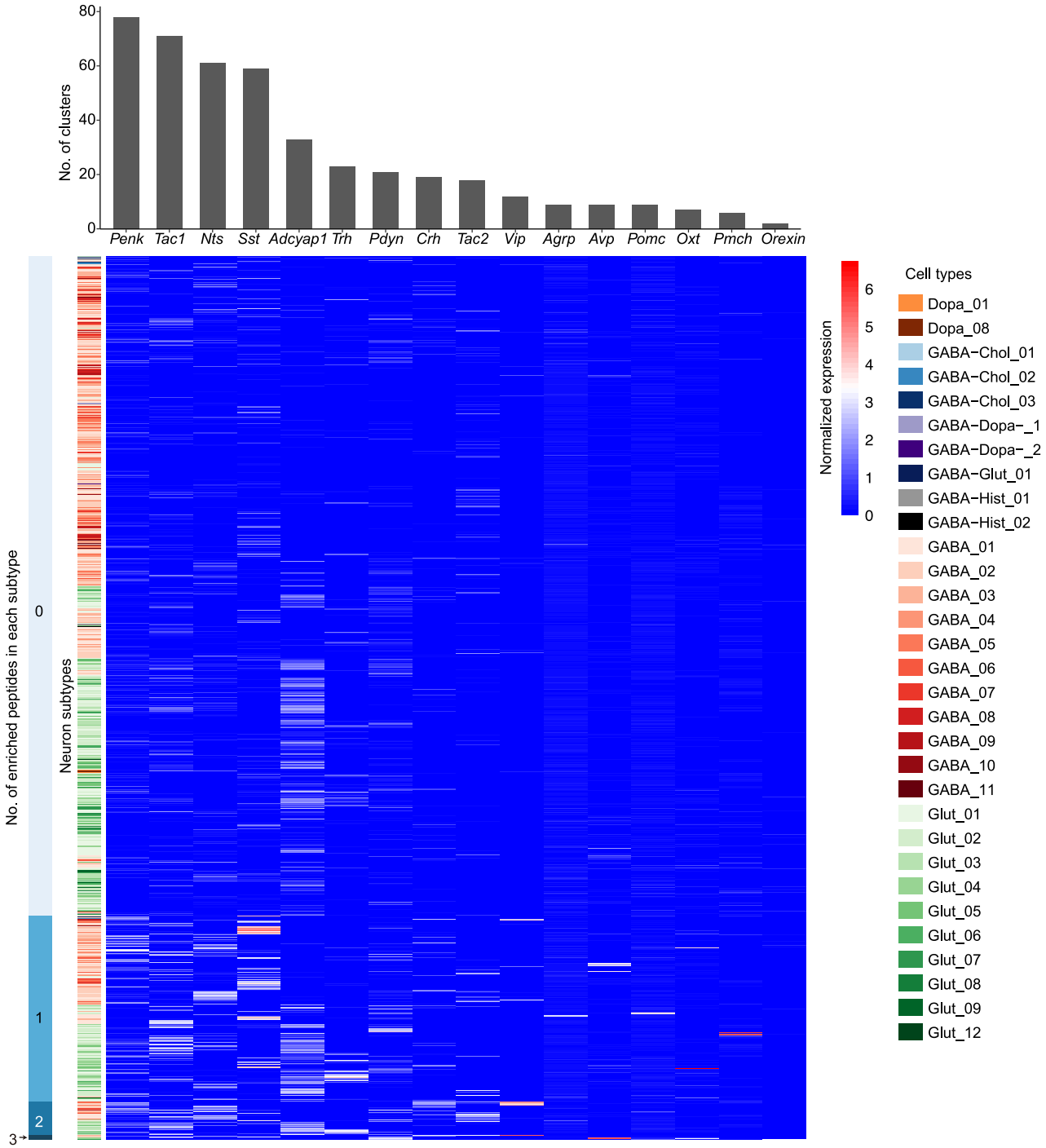

Extended Data Fig. 3 | Transcriptional diversity of hypothalamic peptidergic neuron populations. Heatmap representation of normalized neuropeptide expression (columns) across 1,451 hypothalamic neuron subtypes (rows), referred to as "cell clusters" in the original manuscript[21]. The names of the neuropeptides are indicated above each column. Subtypes are color-coded, labeled on the left, and grouped into 31 cell types, which are color-coded with the legend on the right. A neuropeptide is considered enriched in a cell subtype if more than 25% of neurons within that subtype express it. Among the 1,451 neuron subtypes, 368 showed enrichments for at least one of the 16 neuropeptides: 306 subtypes are enriched for only one neuropeptide, 55 are enriched for two neuropeptides, and 7 are enriched for three neuropeptides.

https://doi.org/10.1038/s41593-025-01919-0

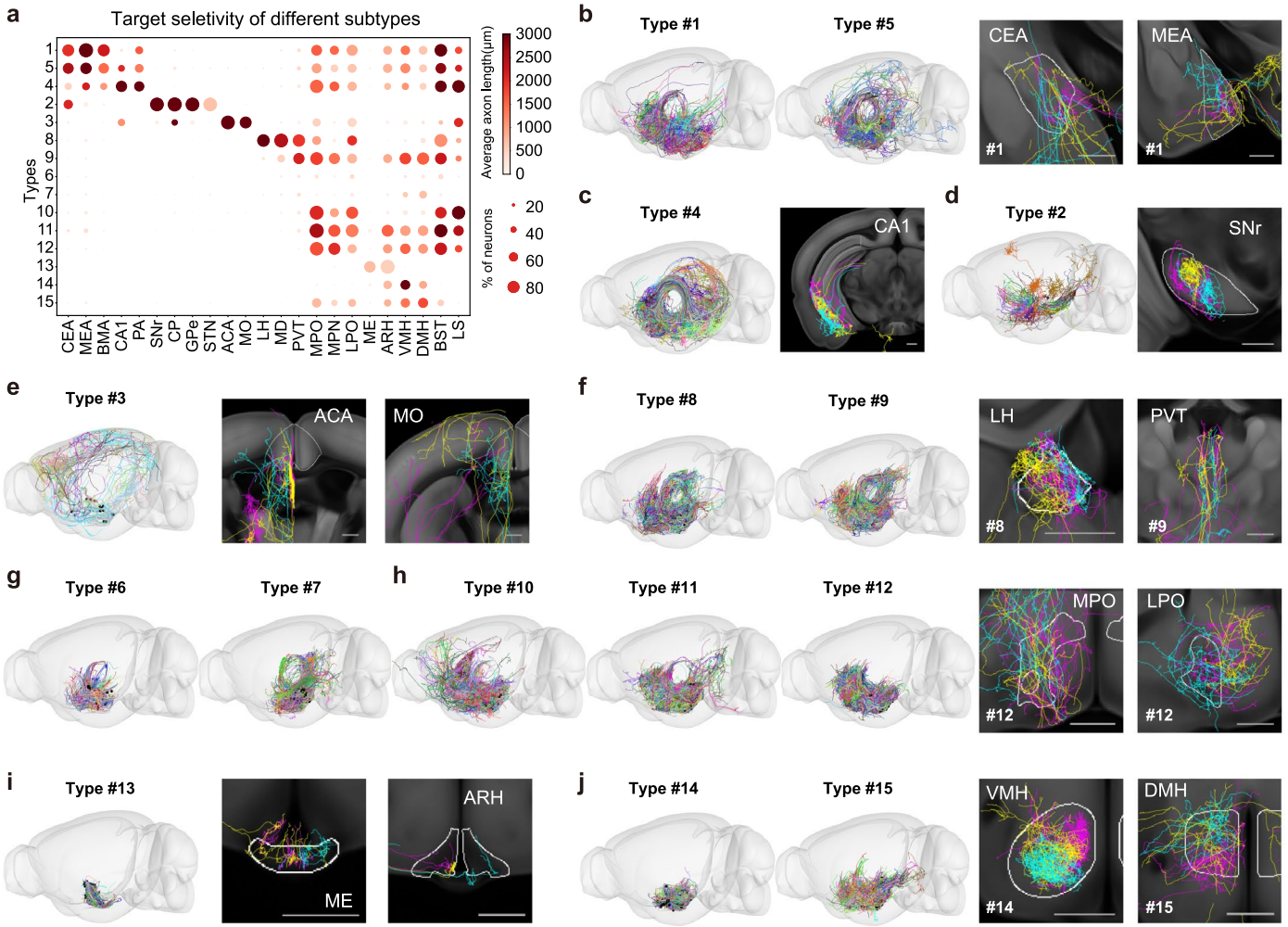

Extended Data Fig. 4 | Characteristics of non-midbrain projecting types 1–15. **a**. A dot plot depicting selective projections of each type (row) in each brain area (column). The size of the dot indicates the percentage of neurons in each type that project to the indicated brain area, and the color intensity represents the average projection length (in μm) in a heatmap fashion, with the scale on the right. **b**–**j**. The total axon projections of neurons of the indicated type are plotted in a 3D brain on the left. Zoom-in views of representative axon projections from three representative neurons (color-coded) from each type in defined subdomains of the indicated target areas are shown on the right. Scale bar, 500 μm.

https://doi.org/10.1038/s41593-025-01919-0

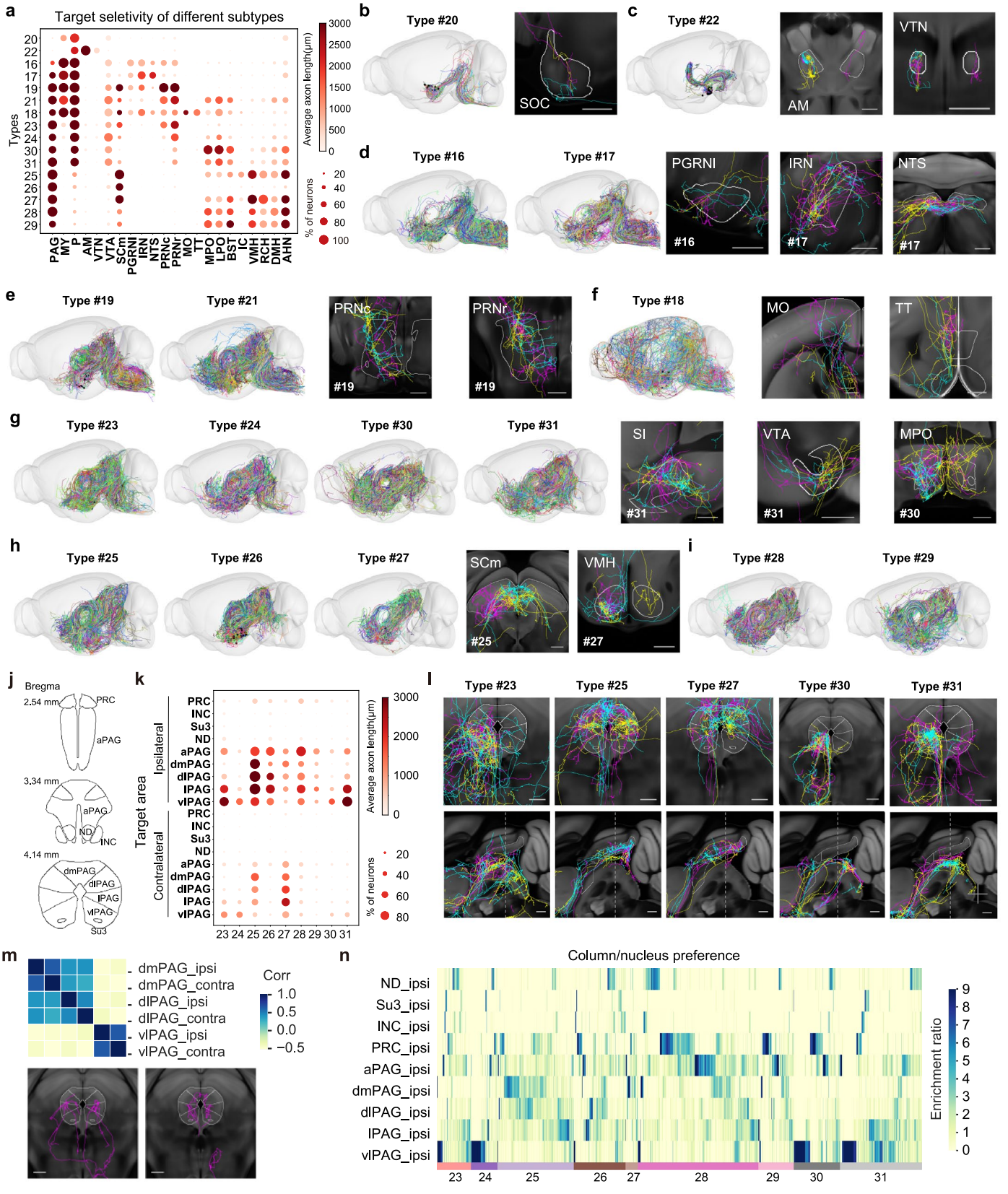

Extended Data Fig. 5 | See next page for caption.

https://doi.org/10.1038/s41593-025-01919-0

Extended Data Fig. 5 | Characteristics of the midbrain projecting types 16–31. **a**. A dot plot depicting selective projections of each type (row) in each brain area (column). The dot circle's size and color intensity indicate the percentage of neurons in each type that project to the indicated brain area and the average projection length (in µm) in a heatmap fashion, respectively, with the scale on the right. **b**–**i**. The total axon projections of neurons of the indicated type are plotted in a 3D brain on the left. Zoom-in views of representative axon projections from three representative neurons (color-coded) from each type in defined subdomains of the indicated target areas are shown on the right. Scale bar, 500 µm. **j**. Schematics showing the nuclei and column structures of the PAG, which includes anterior PAG (aPAG) and rostral nuclei (INC, Su3, ND, and PRC), as well as four longitudinally organized PAG columns - dorsomedial (dm), dorsolateral (dl), lateral (l), and ventrolateral (vl) PAG. **k**. A dot plot depicting selective projections of each type (row) in each PAG column/nucleus on the ipsilateral or contralateral side. The dot circle's size and color intensity indicate the percentage of neurons in each type that project to the indicated brain area and the average projection length (in µm) in each column/nucleus in a heatmap fashion with the scale shown on the right. **l**. Zoom-in views of representative axon projections of three neurons (color-coded) from the indicated type in a coronal (top) and sagittal (bottom) plane of a PAG section. Scale bar, 500 µm. Dashed lines show the position of the coronal section on the sagittal plane. **m**. Correlation (corr) analysis of preference index in the ipsilateral (ipsi) and contralateral side (contra) of the indicated PAG column/nucleus for bilaterally PAG-projecting neurons. Representative images on the bottom show a coordinated innervation pattern of a similar column/nucleus in both hemispheres by two bilaterally PAG-projecting neurons. **n**. Heatmap representation (sorted) of column/nucleus preference score for projections in the ipsilateral PAG, calculated as the fold difference of projection density (total arbor length divided by the volume of targeted area) for a particular column/nucleus relative to the average projection density for all areas, of individual neurons in each type.

https://doi.org/10.1038/s41593-025-01919-0

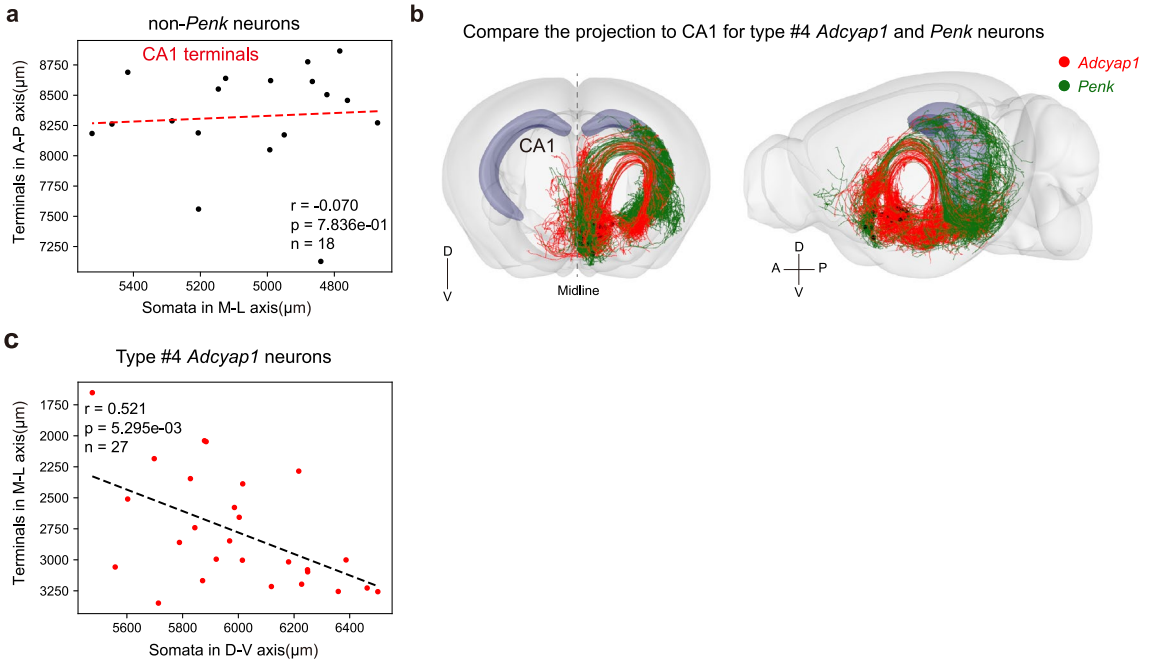

Extended Data Fig. 6 | Topographic arrangements of axon projections of type 4 neurons expressing *Adcyap1* in the ventral CA1. a. No topographic correspondence between the soma and terminal distribution in dorsal CA1 in non-*Penk* type 4 neurons. **b**. *Adcyap1*-expressing type 4 neurons predominantly projected to ventral CA1 while *Penk*-expressing type 4 neurons predominantly projected to dorsal CA1. **c**. Correlation analysis between the soma distribution of *Adcyap1*-expressing type 4 neurons and their termini in ventral CA1 reveals a topographic correspondence between the soma distribution along the D-V axis and their termini distribution along the M-L axis. A linear regression analysis was conducted in panels a and c to examine the relationship between the soma position and the center position of projections in downstream targets along the specified axis. The "r" values represent the regression coefficient, and their significance (*P* values) was evaluated using a two-tailed t-test.

https://doi.org/10.1038/s41593-025-01919-0

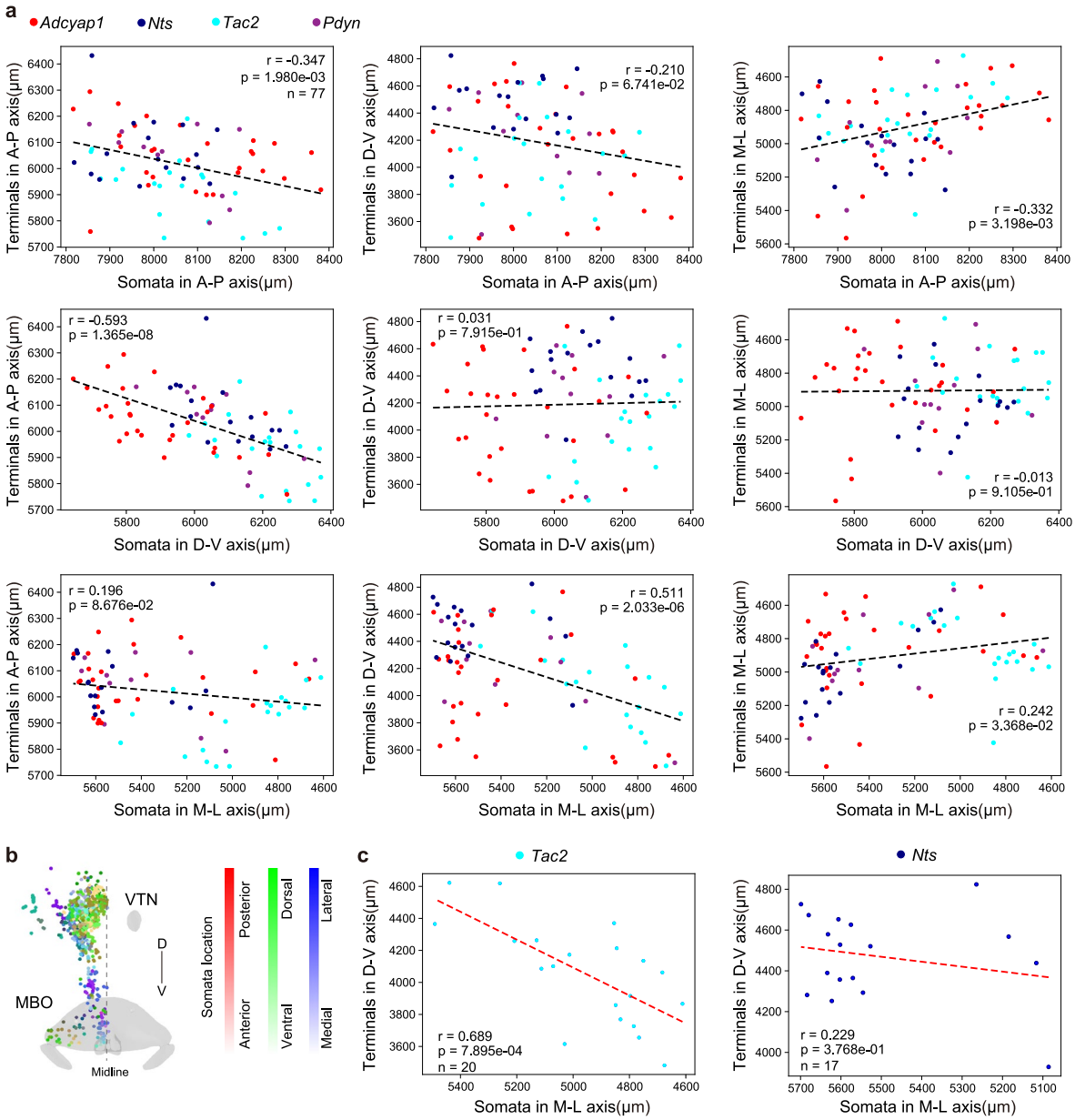

Extended Data Fig. 7 | Complex topographic arrangements of axon projections of type 22 neurons. a. Correlation analysis of the soma distribution of various neuropeptide populations (indicated by colors) within MBO type 22 neurons and their axon terminal distribution in ATN reveals intricate topographic arrangements across all three axes. **b.** Illustration of the collective arrangement of axon collateral projections from all MBO type 22 neurons in and around VTN in reference to the soma locations along the three axes. No discernible topographic correspondence was observed. **c.** Correlation analysis between the soma distribution of specific neuropeptide populations within MBO type 22 neurons along the Medial-Lateral (M-L) axis and their ATN terminals along the Dorsal-Ventral (D-V) axis shows topographic axon arrangements for *Tac2*-expressing neurons but not *Nts*-expressing neurons. A linear regression analysis was conducted in a and c to examine the relationship between the soma position and the center position of projections in downstream targets along the specified axis. The "r" values represent the regression coefficient, and their significance (*P* values) was evaluated using a two-tailed t-test.

https://doi.org/10.1038/s41593-025-01919-0

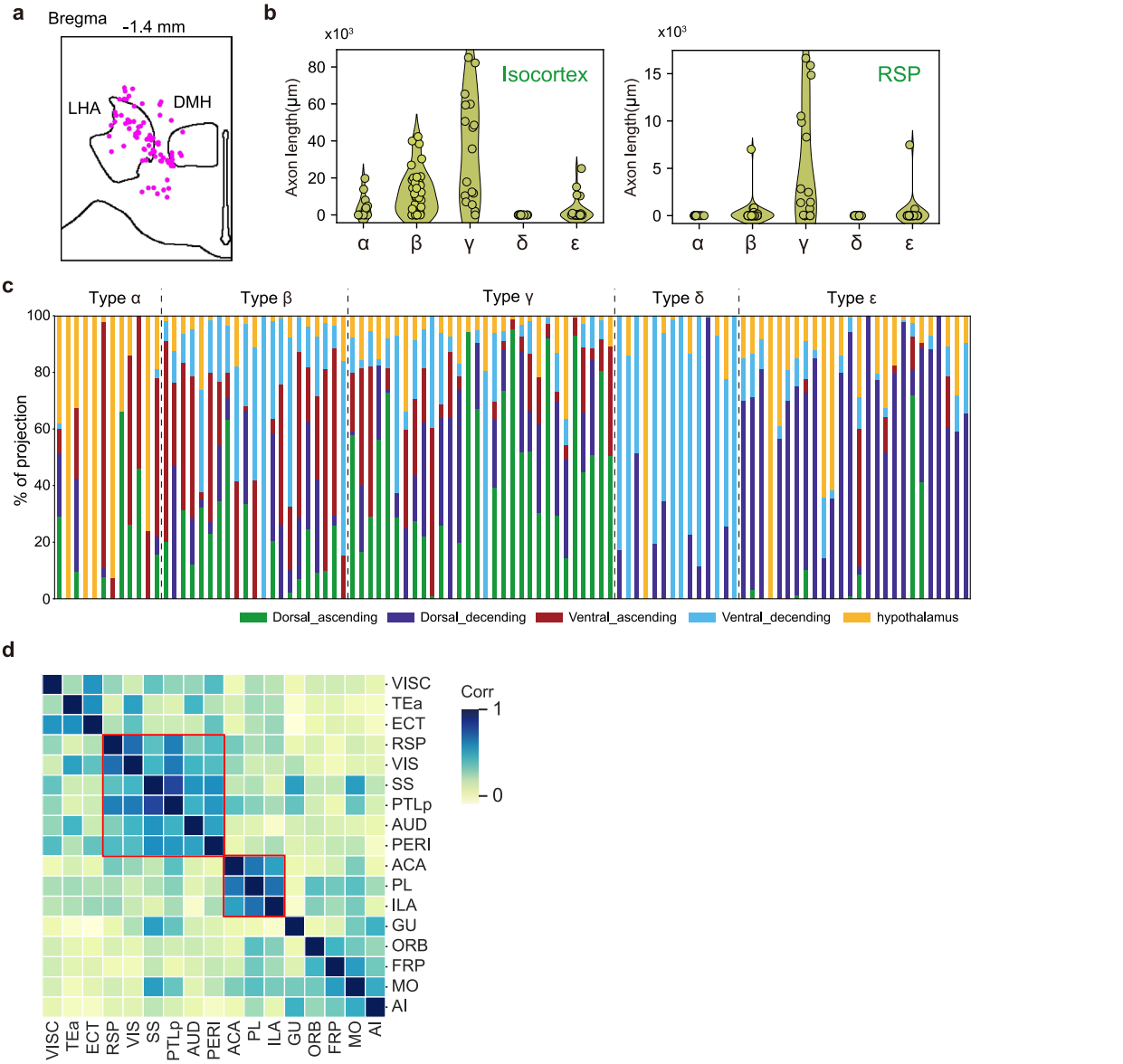

Extended Data Fig. 8 | Characteristics of projectome-defined *Orexin* neuron types. a. Soma locations of LHA *Orexin* neurons from a published MERFISH dataset[21]. These neurons were identified as a single transcriptome-defined type among the 1,451 transcriptionally defined neuronal types found in the hypothalamus. **b**. Violin plots of individual neurons' projection length (in μm) in specific cortical areas for the five projectome types. Each circle represents an individual neuron. **c**. Illustration of the relative distribution of axons from individual *Orexin* neurons within each type across the four designated projecting routes (color-coded). **d**. Correlation (corr) analysis of the projection length of individual *Orexin* neurons in different cortical domains identifies co-innervated areas, as highlighted in red boxes.

https://doi.org/10.1038/s41593-025-01919-0

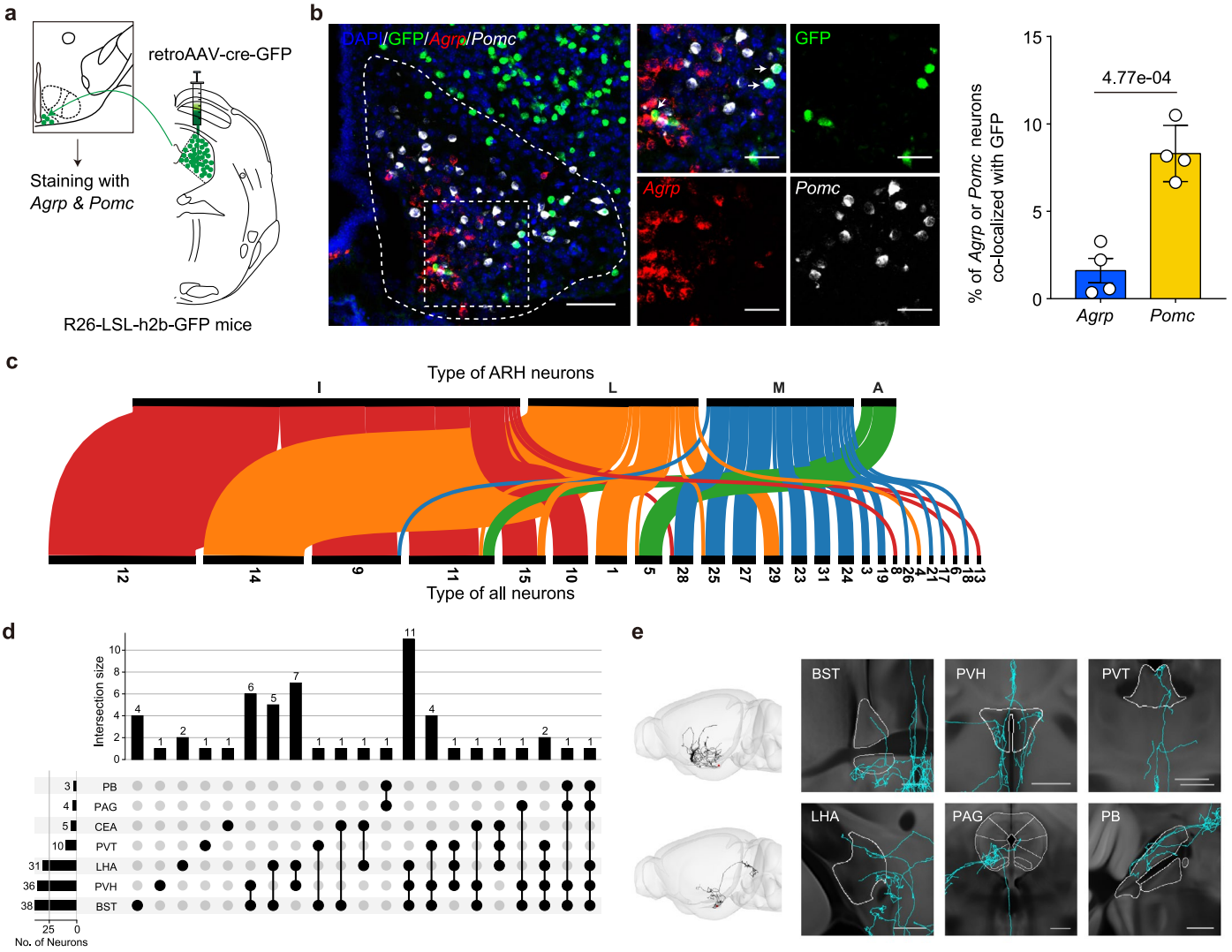

Extended Data Fig. 9 | Axon projections of arcuate *Pomc* and *Agrp* neurons. **a**. Schematics showing the strategy to label PAG-projecting arcuate *Pomc* and *Agrp* neurons by injecting retroAAVs expressing Cre-GFP into a reporter mouse line expressing Cre-inducible histone-GFP. **b**. Representative images and quantification showing a higher percentage of *Pomc* neurons being labeled with GFP with the strategy described in **a**. The fluorescent images show immunostaining of GFP along with florescent in situ signals of *Agrp* and *Pomc*. Regions within the white box are highlighted on the right with zoom-in views. Scale bar, 100 μm. Data are presented as mean ± S.E.M., with individual data points shown as circles. N = 4 for either group. The *P* value above the bar graphs was determined by two-tailed t-test. **c**. Correspondence between *Pomc* and *Agrp* projectomes types and the 31 projectome types defined based on the entire dataset. **d**. An upset plot showing the intersection size of *Agrp* neurons that send axons to multiple brain areas indicated on the left. **e**. Axon projections of two representative *Agrp* neurons in 3D brain view on the left and zoom-in views of axon in the indicated target areas for either neuron on the right. Both neurons project to multiple targets.

https://doi.org/10.1038/s41593-025-01919-0

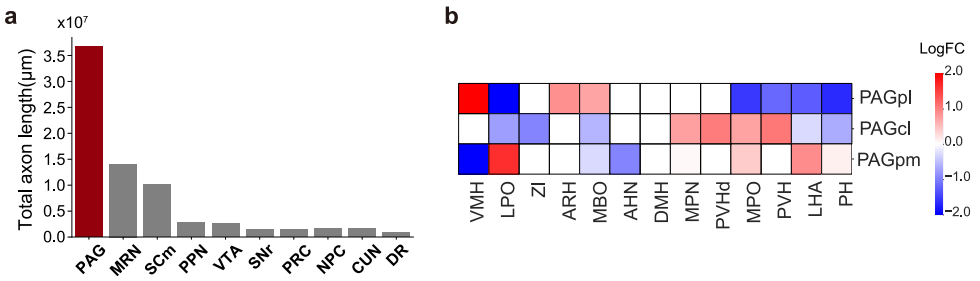

Extended Data Fig. 10 | Prominent PAG projections from hypothalamic Peptidergic Neurons to PAG. a. The total length (in µm) of axon projections from all reconstructed neurons in various midbrain areas demonstrates the highest projection strength observed in PAG. **b**. Heatmap depiction illustrating the enrichment of soma location across indicated hypothalamic nuclei (columns) for the newly defined PAG subdomains (rows). Only log2 fold change (LogFC) values reaching significance ($p < 0.05$) are shown.

nature portfolio

Corresponding author(s): XiaohongXu,YangangSun,Hui Gong,Shengjin Xu,Yidi Sun

Last updated by author(s): Jan 3, 2025

Reporting Summary

Nature Portfolio wishes to improve the reproducibility of the work that we publish. This form provides structure for consistency and transparency in reporting. For further information on Nature Portfolio policies, see our Editorial Policies and the Editorial Policy Checklist.

Statistics

For all statistical analyses, confirm that the following items are present in the figure legend, table legend, main text, or Methods section.

n/a	Confirmed
☐	☒ The exact sample size (*n*) for each experimental group/condition, given as a discrete number and unit of measurement
☐	☒ A statement on whether measurements were taken from distinct samples or whether the same sample was measured repeatedly
☐	☒ The statistical test(s) used AND whether they are one- or two-sided *Only common tests should be described solely by name; describe more complex techniques in the Methods section.*
☒	☐ A description of all covariates tested
☐	☒ A description of any assumptions or corrections, such as tests of normality and adjustment for multiple comparisons
☐	☒ A full description of the statistical parameters including central tendency (e.g. means) or other basic estimates (e.g. regression coefficient) AND variation (e.g. standard deviation) or associated estimates of uncertainty (e.g. confidence intervals)
☐	☒ For null hypothesis testing, the test statistic (e.g. *F*, *t*, *r*) with confidence intervals, effect sizes, degrees of freedom and *P* value noted *Give P values as exact values whenever suitable.*
☒	☐ For Bayesian analysis, information on the choice of priors and Markov chain Monte Carlo settings
☐	☒ For hierarchical and complex designs, identification of the appropriate level for tests and full reporting of outcomes
☐	☒ Estimates of effect sizes (e.g. Cohen's *d*, Pearson's *r*), indicating how they were calculated

Our web collection on statistics for biologists contains articles on many of the points above.

Software and code

Policy information about availability of computer code

Data collection	Customized software,Fast Neurite Tracer was used for image processing and reconstruction of axon morphologies.
Data analysis	Image]v1.52n;National Institutes of Health;https://imagej.nih.gov/j/; RStudio IDEv1.4.1717;RStudio;https://www.rstudio.com; R v4.2.2;R Foundation;https://www.R-project.org; ITK-SNAPv3.6;http://www.itksnap.org/pmwiki/pmwiki.php; MATLAB 2019a;MathWork;https://www.mathworks.com; Python;Python 3.10.10;https://www.python.org/; Customized code:NeuronVis;https://gitee.com/bigduduwxf/neuron-vis; Customized code:pyswcloaderhttps://github.com/txgxxx/pyswcloader; Customized code:https://github.com/xulab2022/Single-Neuron-Projectome-of-Hypothalamus/tree/master;

For manuscripts utilizing custom algorithms or software that are central to the research but not yet described in published literature, software must be made available to editors and reviewers. We strongly encourage code deposition in a community repository (e.g. GitHub). See the Nature Portfolio guidelines for submitting code & software for further information.

Data

Policy information about availability of data

All manuscripts must include a data availability statement. This statement should provide the following information, where applicable:

- Accession codes, unique identifiers, or web links for publicly available datasets
- A description of any restrictions on data availability
- For clinical datasets or third party data, please ensure that the statement adheres to our policy

All data can be visualized and downloaded from the website:https://mouse.digital-brain.cn/projectome/hy.

Research involving human participants, their data, or biological material

Policy information about studies with human participants or human data. See also policy information about sex, gender (identity/presentation), and sexual orientation and race, ethnicity and racism.

Reporting on sex and gender	NA
Reporting on race, ethnicity, or other socially relevant groupings	NA
Population characteristics	NA
Recruitment	NA
Ethics oversight	NA

Note that full information on the approval of the study protocol must also be provided in the manuscript.

Field-specific reporting

Please select the one below that is the best fit for your research. If you are not sure, read the appropriate sections before making your selection.

☒ Life sciences ☐ Behavioural & social sciences ☐ Ecological, evolutionary & environmental sciences

For a reference copy of the document with all sections, see nature.com/documents/nr-reporting-summary-flat.pdf

Life sciences study design

All studies must disclose on these points even when the disclosure is negative.

Sample size	We reconstructed 7180 neurons hypothalamic peptidergic neurons in this study (At least two mice have undergone fMOST imaging for each peptide).
Data exclusions	All neurons were manually checked to ensure that they were correctly traced. Neuron found to have erroneous tracing were excluded from further analysis.
Replication	All tracing data were collected from 166 samples. Each peptidergic neuron type was collected from at least two mice. The detailed information could be found in Supplementary Table 1.
Randomization	This study did not involve allocation of experimental groups.
Blinding	Tracing staffs were blind to the information of neurons (e.g. soma location, peptidergic types).

Reporting for specific materials, systems and methods

We require information from authors about some types of materials, experimental systems and methods used in many studies. Here, indicate whether each material, system or method listed is relevant to your study. If you are not sure if a list item applies to your research, read the appropriate section before selecting a response.

Materials & experimental systems

n/a	Involved in the study
☐	☒ Antibodies
☒	☐ Eukaryotic cell lines
☒	☐ Palaeontology and archaeology
☐	☒ Animals and other organisms
☒	☐ Clinical data
☒	☐ Dual use research of concern
☒	☐ Plants

Methods

n/a	Involved in the study
☒	☐ ChIP-seq
☒	☐ Flow cytometry
☒	☐ MRI-based neuroimaging

Antibodies

Antibodies used	Anti-GFP antibody (ab13970) 1:300 dilution
Validation	https://www.abcam.cn/products/primary-antibodies/gfp-antibody-ab13970.html

Animals and other research organisms

Policy information about studies involving animals; ARRIVE guidelines recommended for reporting animal research, and Sex and Gender in Research

Laboratory animals	Transgenic mice or C57BL/6J wild type mice. Detailed information of strain and age can be found in Supplementary Table 1. Mice were raised under the standard condition (12-hr light/dark cycle, 22-25°C, 30-70% humidity) with the access to food and water ad libitum.
Wild animals	The study did not involve wild animals.
Reporting on sex	We only use male mice in this study.
Field-collected samples	The study did not involve samples collected from the field.
Ethics oversight	Animal experimental procedures and care were approved by the Animal Care and Use Committee of the Center for Excellence in Brain Science and Intelligence Technology (Institute of Neuroscience), Chinese Academy of Sciences, Shanghai, China.

Note that full information on the approval of the study protocol must also be provided in the manuscript.

Plants

Seed stocks	NA
Novel plant genotypes	NA
Authentication	NA